

Statistical and analytical approaches to finite-temperature magnetic properties of the compound SmFe_{12}

Takuya Yoshioka and Hiroki Tsuchiura

Department of Applied Physics, Tohoku University, Sendai 980-8579, Japan;
ESICMM, National Institute for Materials Science, Tsukuba, Ibaraki 305-0047, Japan;
and Center for Spintronics Research Network, Tohoku University, Sendai 980-8577, Japan

Pavel Novák

Institute of Physics of ASCR, Cukrovarnická, Prague 6 162 00, Czech Republic



(Received 2 September 2020; accepted 26 October 2020; published 10 November 2020)

To investigate the magnetic properties of SmFe_{12} , we construct an effective spin model, where magnetic moments, crystal-field (CF) parameters, and exchange fields at 0 K are determined by first-principles calculations. Finite-temperature magnetic properties are investigated by using this model. We further develop an analytical method with strong mixing of states with a different quantum number of angular momentum J (J -mixing), which is caused by a strong exchange field acting on the spin component of $4f$ electrons. Comparing our analytical results with those calculated by Boltzmann statistics, we clarify that the previous analytical studies for Sm transition-metal compounds overestimate the J -mixing effects. The present method enables us to perform a quantitative analysis of the temperature dependence of magnetic anisotropy (MA) with high reliability. The analytical method with model approximations reveals that the J -mixing caused by the exchange field increases the spin angular momentum, which enhances the absolute value of the orbital angular momentum and MA constants via spin-orbit interaction. It is also clarified that these J -mixing effects remain even above room temperature. Magnetization of SmFe_{12} shows a peculiar field dependence known as the first-order magnetization process (FOMP), where the magnetization shows an abrupt change at a certain magnetic field. The result of the analysis shows that the origin of FOMP is attributed to competitive MA constants between positive K_1 and negative K_2 . The sign of $K_{1(2)}$ appears due to an increase in the CF potential denoted by the parameter $A_2^0(r^2)$ ($A_4^0(r^4)$) caused by hybridization between $3d$ -electrons of Fe on the $8i$ ($8j$) site and $5d$ and $6p$ valence electrons on the Sm site. It is verified that the requirement for the appearance of FOMP is given as $-K_2 < K_1 < -6K_2$.

DOI: [10.1103/PhysRevB.102.184410](https://doi.org/10.1103/PhysRevB.102.184410)

I. INTRODUCTION

There have been intensive studies on developing new rare-earth (R) lean permanent magnetic materials that have strong magnetic properties comparable to those of Nd-Fe-B. Nitrogenated compounds such as NdFe_{12}N or $\text{NdFe}_{11}\text{TiN}$ have been considered to be candidates of such materials, and thus a series of experimental and theoretical efforts have been made to figure out the magnetic properties of these materials [1,2]. SmFe_{12} with the ThMn_{12} structure (Fig. 1) is also a possible candidate and has attracted renewed interest because it exhibits excellent intrinsic magnetic properties such as uniaxial magnetocrystalline anisotropy [3]. Although SmFe_{12} itself is thermodynamically unstable, it has been known that the substitution of Fe with a stabilizing element, such as Ti or V, can remove this difficulty [4–8]. In these systems, however, the saturated magnetization is reduced due to antiparallel alignment of magnetic moments of Ti and V relative to those of Fe. The recent development of synthesis technology made it possible to fabricate highly textured single-phase samples of SmFe_{12} thin film [9–13], and it has been shown experimentally that Co substitution for Fe enhances their magnetic

properties, such as Curie temperature and magnetic anisotropy (MA) [10]. Thus, SmFe_{12} -based systems belong to one of the most promising hard magnetic materials, and therefore it is crucially important to clarify the basic magnetic properties of SmFe_{12} .

So far, many attempts have been made to gain a microscopic understanding of the magnetic properties of R -based permanent magnets [14–19]. Among them, a powerful method is to combine the first-principles calculations for electronic states at the ground state with a suitable model for finite-temperature properties [20–29]. With regard to SmFe_{12} , Harashima *et al.* [30], Körner *et al.* [31], and Delonge *et al.* [32] performed the first-principles calculations and model analysis of magnetic properties. In the theoretical study of Sm-based intermetallic compounds, however, there remains a basic issue of how to deal with the formidably strong J -mixing effects in Sm. This is the problem that has been studied for a long period on Sm-based magnets [33–35]. There have been some attempts to include J -mixing in the analytical form via first-order perturbation for crystal fields (CFs) [28,29]. However, Kuz'min pointed out that the Sm-based magnetic materials are exceptional for application of the method [28].

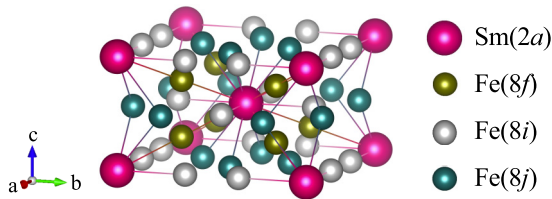


FIG. 1. Crystal structure of SmFe_{12} in ThMn_{12} structure. In-equivalent sites: $\text{Sm}(2a)$, $\text{Fe}(8f)$, $\text{Fe}(8i)$, and $\text{Fe}(8j)$ are shown by different-colored balls, and solid lines show interatomic short contacts less than 3.2 Å.

We have recently developed a similar method [18,19], in which the model parameters are calculated by first-principles calculations, and the finite-temperature magnetic properties are calculated in a statistical way, and we applied our method to $R_2\text{Fe}_{14}\text{B}$ systems. By taking into account CF parameters up to sixth order, the model satisfactorily explained the experimental results for magnetization curves and the temperature dependence of MA constants [18,19]. Using the method, we recently calculated the temperature dependence of the MA constants of SmFe_{12} and showed that $K_1 > 0$ and $K_2 < 0$, in agreement with experimental results [12]. The report of the work, however, contains only the final results, and no details of the computational procedure have been presented. As a result, no explanations have been given of the mechanism for the results $K_1 > 0$ and $K_2 < 0$.

The purpose of the present study is thus to clarify the origin of the finite-temperature magnetic properties of SmFe_{12} using statistical and analytical approaches. To this end, we develop statistical and analytical methods based on first-principles calculations. The analytical procedure is able to derive simple relations between the temperature dependence of magnetic properties and parameters determined by first-principles electronic structure calculations. The treatment of the J -mixing effects adopted previously by other groups [28,29] will be modified, and the results will be compared with the statistical results of the temperature dependence of the magnetic properties of SmFe_{12} . Good agreement between the analytical and statistical results guarantees the applicability of the modified analytical formula to Sm compounds.

In the following we present the model Hamiltonian, the parameters of which are determined by first-principles calculations, and we present the calculation procedure for finite temperatures, especially the statistical method, to obtain the MA constants and magnetization curves, and to explain the modified analytical method. The latter method may clarify the relations among the free energy of the system, the CF, and the exchange field. Using the analytical method, we will show that the mechanism of $K_1 > 0$ and $K_2 < 0$ in SmFe_{12} is attributed to the characteristic lattice structure around Sm ions, that is, crystallographic $2b$ -sites on the c -axis adjacent to Sm are vacant. We also present results on the magnetization process and nucleation fields by calculating Gibbs free energy. As pointed out in Ref. [19], this analytical spin model can be easily extended to Sm ions around the intergranular phases, which is crucially important in the coercivity mechanism [13,36,37].

This paper is organized as follows. The model Hamiltonian is explained in Sec. II, and the procedures of the statistical and

analytical methods are explained in Sec. III. Section IV shows the results of the temperature dependence of magnetic properties calculated using the statistical and analytical methods. A summary of our work is given in Sec. V.

II. MODEL HAMILTONIAN

We adopt the following Hamiltonian to investigate the magnetic properties of R transition-metal (TM) compounds:

$$\hat{\mathcal{H}} = \frac{1}{V_0} \sum_{j=1}^{n_R} \hat{\mathcal{H}}_{R,j} + K_1^{\text{TM}}(T) \sin^2 \theta^{\text{TM}} - \mathbf{M}^{\text{TM}}(T) \cdot \mathbf{B}, \quad (1)$$

where $\hat{\mathcal{H}}_{R,j}$ is a Hamiltonian for the R ion on the j th site, and n_R is the number of R ions in the unit-cell volume V_0 . The second and third terms represent the phenomenological treatment of MA energy and the Zeeman term on the TM sublattice, where $K_1^{\text{TM}}(T)$ and $\mathbf{M}^{\text{TM}}(T)$ are the temperature-dependent anisotropy constant and magnetization vector of the TM sublattice, respectively, and θ^{TM} is the polar angle of $\mathbf{M}^{\text{TM}}(T)$ against the c -axis. $\mathbf{M}^{\text{TM}}(T)$ is given as $M^{\text{TM}}(T)\mathbf{e}^{\text{TM}}$ by using the absolute value of the sublattice magnetization $M^{\text{TM}}(T)$ and a directional vector \mathbf{e}^{TM} of $\mathbf{M}^{\text{TM}}(T)$. $M^{\text{TM}}(T)$ is defined by a part of the magnetization subtracting the $4f$ electron contribution from the total magnetization. \mathbf{B} is an applied field.

A. Hamiltonian of a single R ion

The Hamiltonian for the $4f$ shell in the j th R ion in Eq. (1) is

$$\hat{\mathcal{H}}_{R,j} = \sum_{i=1}^{n_{4f}} \hat{h}_j(i) + \frac{1}{8\pi\epsilon_0} \sum_{i \neq i'=1}^{n_{4f}} \frac{e^2}{|\hat{\mathbf{r}}_i - \hat{\mathbf{r}}_{i'}|}, \quad (2)$$

with

$$\hat{h}_j(i) = \xi \hat{\mathbf{l}}_i \cdot \hat{\mathbf{s}}_i + 2\mu_B \hat{\mathbf{s}}_i \cdot \mathbf{B}_{\text{ex},j}(T) + \int r_i^2 |R_{4f}(r_i)|^2 V_j(\mathbf{r}_i) dr_i + \mu_B (\hat{\mathbf{l}}_i + 2\hat{\mathbf{s}}_i) \cdot \mathbf{B}. \quad (3)$$

The first and second terms in Eq. (2) represent the single-electron contribution and the electron-electron repulsion in a $4f$ shell, respectively, where n_{4f} is the number of $4f$ electrons, and ϵ_0 and e are the vacuum permittivity and the elementary charge, respectively. $\hat{h}_j(i)$ in Eq. (3) is the Hamiltonian for the i th $4f$ electron on the j th R site, where the first term in Eq. (3) is the spin-orbit interaction (SOI) between spin ($\hat{\mathbf{s}}_i$) and orbital ($\hat{\mathbf{l}}_i$) angular momenta, with a coupling constant ξ . The second term represents the exchange interaction between spin moment and temperature-dependent exchange field $\mathbf{B}_{\text{ex},j}(T) = -e^{\text{TM}} B_{\text{ex},j}(T)$ on the j th R site, where μ_B is the Bohr magneton. The third and fourth terms are the CF and Zeeman terms, respectively. In the expression of CF, $V_j(\mathbf{r}_i)$ and $R_{4f}(r_i)$ are the Coulomb potential and the radial parts of the $4f$ wave function on the j th R site, respectively. Note that the kinetic energy and screened central potential terms are effectively taken into account in the formation of the $4f$ orbital.

To obtain the electronic properties at $T = 0$, we apply the first-principles calculations and determine the parameters in

TABLE I. Values of CF potentials $A_{l,j}^m\langle r^l \rangle$ (K), exchange field $\mu_B B_{\text{ex},j}(0)/k_B$ (K), and TM-sublattice magnetization $V_0 M^{\text{TM}}(0)$ (μ_B) in SmFe_{12} calculated by first-principles calculations, where μ_B and k_B are the Bohr magneton and Boltzmann constant, respectively, and $V_0 = a \times b \times c$. We note that $A_{l,j}^m\langle r^l \rangle$ and $\mu_B B_{\text{ex},j}(0)/k_B$ are independent of site index j .

$A_{2,j}^0\langle r^2 \rangle$	$A_{4,j}^0\langle r^4 \rangle$	$A_{4,j}^4\langle r^4 \rangle$	$A_{6,j}^0\langle r^6 \rangle$	$A_{6,j}^4\langle r^6 \rangle$	$\mu_B B_{\text{ex},j}(0)/k_B$	$V_0 M^{\text{TM}}(0)$
-71.4	-21.3	-49.3	5.9	3.0	296.1	51.6

the Hamiltonians in Eq. (3). We use the full-potential linearized augmented plane wave plus local orbitals (APW+lo) method implemented in the WIEN2K code [38]. The Kohn-Sham equations are solved within the generalized-gradient approximation (GGA). To simulate localized $4f$ states, we treat $4f$ states as atomiclike core states, which is the so called open-core method [39–44].

We calculate the ground-state properties of SmFe_{12} such as the Coulomb potential, charge distribution, and sublattice magnetizations. In accord with the previous theoretical studies for SmFe_{12} [30–32], we assume that the Sm ion has a trivalentlike electronic structure. The exchange fields $B_{\text{ex},j}(0)$ at $T = 0$ are determined from an energy increase caused by spin flip of $4f$ electrons [18,45], and CFs acting on the i th $4f$ electron are directly estimated from the Coulomb potential $V_j(\mathbf{r}_i)$ acting on the j th R site. It is noted that the single-ion Hamiltonian $\hat{H}_{R,j}$ thus determined for the j th R ions includes effects of TM atoms surrounding the R ions as a mean field.

Practically, the CF term is rewritten as the following formula [40,42]:

$$\int_0^{r_c} r_i^2 |R_{4f}(r_i)|^2 V_j(\mathbf{r}_i) dr_i = \sum_{l,m} \frac{A_{l,j}^m\langle r^l \rangle}{a_{l,m}} t_l^m(\hat{\theta}_i, \hat{\varphi}_i), \quad (4)$$

$$A_{l,j}^m\langle r^l \rangle = a_{l,m} \int_0^{r_c} dr_i r_i^2 |R_{4f}(r_i)|^2 \times \int d\Omega_i V_j(\mathbf{r}_i) t_l^m(\theta_i, \varphi_i), \quad (5)$$

where $A_{l,j}^m\langle r^l \rangle$ is the CF parameter on the j th R site, $a_{l,m}$ is a numerical factor [46], $t_l^m(\hat{\theta}_i, \hat{\varphi}_i)$ is a tesseral harmonic function of a solid angle $\Omega = (\hat{\theta}_i, \hat{\varphi}_i)$, and r_c is a cutoff radius.

Values of CF parameters $A_{l,j}^m\langle r^l \rangle$ in Eq. (5), exchange field $B_{\text{ex},j}(0)$ in Eq. (3), and TM-sublattice magnetization $M^{\text{TM}}(0)$ in Eq. (1) in SmFe_{12} are shown in Table I. The lattice constants used in these calculations are the experimental values $a = b = 8.35 \text{ \AA}$ and $c = 4.8 \text{ \AA}$ [10]. For Wyckoff positions, we apply the theoretically optimized ones given in Ref. [30]. The crystal structure of SmFe_{12} is shown in Fig. 1.

B. Single R ion Hamiltonian in the LS coupling regime

We apply the concept of LS coupling to the single-electron Hamiltonian of Eq. (3) with Russell Saunders states $|L, S; J, M\rangle$, due to the strong Coulomb interaction between $4f$ electrons. According to Hund's rule, we specify the quantum number of the total orbital (spin) moment $L(S)$. Total angular momentum J is varied from $|L - S|$ to $L + S$, and M is the magnetic quantum number. Thus the single-ion

Hamiltonian in Eq. (2) can be reduced to

$$\hat{H}_R = \hat{H}_{\text{so}} + \hat{H}_{\text{ex}} + \hat{H}_{\text{CF}} + \hat{H}_Z, \quad (6)$$

$$\hat{H}_{\text{so}} = \lambda \hat{\mathbf{L}} \cdot \hat{\mathbf{S}}, \quad (7)$$

$$\hat{H}_{\text{ex}} = 2\mu_B \hat{\mathbf{S}} \cdot \mathbf{B}_{\text{ex}}(T), \quad (8)$$

$$\hat{H}_{\text{CF}} = \sum_{l,m,m'} B_l^m \Theta_l^L C_m^{(l)}(\hat{\mathbf{L}}), \quad (9)$$

$$\hat{H}_Z = \mu_B (\hat{\mathbf{L}} + 2\hat{\mathbf{S}}) \cdot \mathbf{B}. \quad (10)$$

Hereafter, the site index j is omitted for a single-ion quantity. $\hat{\mathbf{L}}$ and $\hat{\mathbf{S}}$ are total orbital and spin momenta of $4f$ electrons, respectively, $B_l^0 = \sqrt{(2l+1)/4\pi} A_l^0\langle r^l \rangle / a_{l,0}$ and $B_l^{\pm|m|} = (\mp 1)^m \sqrt{(2l+1)/8\pi} [A_l^{|m|}\langle r^l \rangle \mp i A_l^{-|m|}\langle r^l \rangle] / a_{l,m}$ for $m \neq 0$, and $\Theta_l^L = \langle L \| \sum_i C_m^{(l)}(\hat{\theta}_i, \hat{\varphi}_i) \| L \rangle / \langle L \| \sum_i C_m^{(l)}(\hat{\mathbf{L}}) \| L \rangle$. In the treatment of SOI, we should note that the eigenstates of LS coupling are specified by the quantum number of J . In general, the term \hat{H}_{so} is dominating in Eq. (6). Thus J is a good quantum number in most of the R - $4f$ systems. Because the LS coupling in Sm compounds is weak compared with other R ones, it is necessary to include excited J -multiplets. Hereafter, we abbreviate the states $|L, S; J, M\rangle$ as $|J, M\rangle$.

The energy levels of Sm- $4f$ states in SmFe_{12} depend on $B_{\text{ex}}(T)$ and applied field \mathbf{B} . Figure 2 shows the $B_{\text{ex}}(T)/B_{\text{ex}}(0)$ dependence of the energy levels for $e^{\text{TM}} = n_c$, which is a unit vector parallel to the c -axis, and for $\mathbf{B} = \mathbf{0}$. The data needed are given in Table I. As for the SOI constant, we use an experimental value of $\lambda/k_B = \xi/5k_B = 411 \text{ K}$ [47]. At $B_{\text{ex}}(T) = 0$ the S is strongly coupled with L to form a Kramers doublet with a total angular momentum J due to the large LS coupling with fine CF splitting. With increasing $B_{\text{ex}}(T)/B_{\text{ex}}(0)$, the

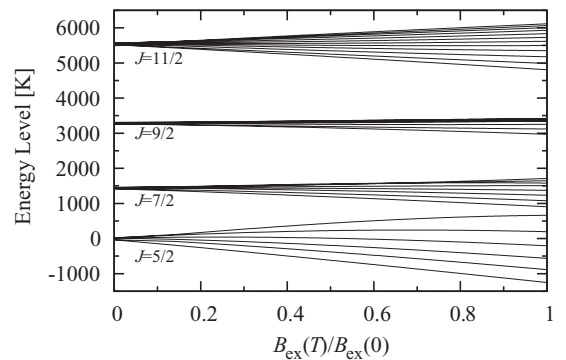


FIG. 2. Energy levels as a function of $B_{\text{ex}}(T)/B_{\text{ex}}(0)$ of the Sm- $4f$ states in SmFe_{12} at $e^{\text{TM}} = n_c$ and for $\mathbf{B} = \mathbf{0}$. High-energy levels originating from $J = 13/2$ and $15/2$ multiplets are above 6000 K, which are not shown.

exchange field breaks the time-reversal symmetry and lift the degeneracy.

C. Phenomenological model for the TM sublattice

For finite-temperature magnetic properties of TM, we apply a phenomenological formula assuming uniform $M^{\text{TM}}(T)$ and $K_1^{\text{TM}}(T)$. For $M^{\text{TM}}(T)$, we apply the Kuz'min formula [48]:

$$\frac{M^{\text{TM}}(T)}{M^{\text{TM}}(0)} = \frac{B_{\text{ex}}(T)}{B_{\text{ex}}(0)} = \alpha(T), \quad (11)$$

$$\alpha(T) = \left[1 - s \left(\frac{T}{T_C} \right)^{3/2} - (1-s) \left(\frac{T}{T_C} \right)^{5/2} \right]^{1/3}, \quad (12)$$

where T_C is the Curie temperature and s is a fitting parameter. The temperature dependence of $K_1^{\text{TM}}(T)$ has been expressed by an extended power law [23]:

$$\begin{aligned} \frac{K_1^{\text{TM}}(T)}{K_1^{\text{TM}}(0)} &= \alpha^3(T) + \frac{8}{7} C_1 [\alpha^3(T) - \alpha^{10}(T)] \\ &+ \frac{8}{7} C_2 \left[\alpha(T)^3 - \frac{18}{11} \alpha(T)^{10} + \frac{7}{11} \alpha(T)^{21} \right], \end{aligned} \quad (13)$$

where C_1 and C_2 are fitting parameters.

In the present study for SmFe₁₂, we use values of $s = 0.01$ and $T_C = 555$ K in Eq. (12), as used by Hirayama *et al.* [10]. They showed that the magnetization agrees well with experimental measurement for SmFe₁₂. The values of C_1 , C_2 , and $V_0 K_1^{\text{TM}}(0)$ in Eq. (13) are determined as -0.263 , -0.237 , and 47.7 K, respectively, by fitting the expression to observed data for YFe₁₁Ti in Ref. [49].

III. METHOD OF MODEL CALCULATIONS

A. Statistical method

To calculate the finite-temperature magnetic properties, we use the model Hamiltonian and calculate MA and the magnetic moment for Sm $4f$ electrons using the statistical method for the partial system. Using the eigenvalues of the Hamiltonian Eq. (6), we express the free-energy density as

$$\begin{aligned} G(\mathbf{e}^{\text{TM}}, T, \mathbf{B}) &= \frac{1}{V_0} \sum_{j=1}^{n_R} g_j(\mathbf{e}^{\text{TM}}, T, \mathbf{B}) \\ &+ K_1^{\text{TM}}(T) \sin^2 \theta^{\text{TM}} - \mathbf{B} \cdot \mathbf{M}^{\text{TM}}(T), \end{aligned} \quad (14)$$

$$g_j(\mathbf{e}^{\text{TM}}, T, \mathbf{B}) = -k_B T \ln Z_j(\mathbf{e}^{\text{TM}}, T, \mathbf{B}), \quad (15)$$

$$Z_j(\mathbf{e}^{\text{TM}}, T, \mathbf{B}) = \sum_n \exp \left[-\frac{E_{n,j}(\mathbf{e}^{\text{TM}}, T, \mathbf{B})}{k_B T} \right], \quad (16)$$

where $g_j(\mathbf{e}^{\text{TM}}, T, \mathbf{B})$ is the Gibbs free energy for R - $4f$ partial system, and $E_{n,j}(\mathbf{e}^{\text{TM}}, T, \mathbf{B})$ and $Z_j(\mathbf{e}^{\text{TM}}, T, \mathbf{B})$ are the eigenvalue and the partition function of the j th R Hamiltonian $\hat{H}_{R,j}$ [Eq. (6)] for given \mathbf{e}^{TM} , respectively. The direction of the TM magnetization \mathbf{e}^{TM} is treated as an external parameter. The equilibrium condition of the system for given T and \mathbf{B} is

$$G(\mathbf{e}_0^{\text{TM}}, T, \mathbf{B}) = \min_{\mathbf{e}^{\text{TM}}} G(\mathbf{e}^{\text{TM}}, T, \mathbf{B}), \quad (17)$$

where \mathbf{e}_0^{TM} is the direction of TM sublattice magnetization in the equilibrium. In practice, we determine the minimal $G(\mathbf{e}^{\text{TM}}, T, \mathbf{B})$ numerically by changing \mathbf{e}^{TM} .

The MA energy is given by the free energy $G(\mathbf{e}^{\text{TM}}, T, \mathbf{0})$ with different directional vector \mathbf{e}^{TM} . In the tetragonal symmetry, $g_j(\mathbf{e}^{\text{TM}}, T, \mathbf{0})$ in $G(\mathbf{e}^{\text{TM}}, T, \mathbf{0})$ is formally expressed as [23,24]

$$\begin{aligned} g_j(\mathbf{e}^{\text{TM}}, T, \mathbf{0}) &= \sum_{p=1}^{\infty} \left[k_{p,j}(T) + \sum_{q=1}^{\lfloor p/2 \rfloor} k_{p,j}^q(T) \cos(4q\varphi^{\text{TM}}) \right] \\ &\times \sin^{2p} \theta^{\text{TM}} + C(T), \end{aligned} \quad (18)$$

where θ^{TM} and φ^{TM} are polar and azimuthal angles of \mathbf{e}^{TM} , respectively, $\lfloor p/2 \rfloor$ indicates the greatest integer of $p/2$, and $k_{p,j}(T)$ and $k_{p,j}^q(T)$ are out-of-plane and in-plane MA constants for the j th R ion. The $C(T)$ is an angle-independent constant. The series expansion does not guarantee convergence [25,26]; however, for finite p , $k_{p,j}^q(T)$ can be obtained from a comparison between Taylor series of $g_j(\mathbf{e}^{\text{TM}}, T, \mathbf{0})$ of Eqs. (15) and (18) with respect to θ^{TM} for a fixed φ^{TM} [21,22] as

$$\begin{aligned} g_j(\mathbf{e}^{\text{TM}}, T, \mathbf{0}) &= g_j^{(0)}(T) + g_j^{(1)}(T) \theta^{\text{TM}} \\ &+ \frac{1}{2!} g_j^{(2)}(T) (\theta^{\text{TM}})^2 + \dots, \\ g_j^{(n)}(T) &= \left. \frac{\partial^n g_j(\theta^{\text{TM}}, \varphi^{\text{TM}}, T, \mathbf{0})}{\partial (\theta^{\text{TM}})^n} \right|_{\substack{\theta^{\text{TM}}=0 \\ \varphi^{\text{TM}}=\pi/8}}, \end{aligned}$$

and

$$\begin{aligned} g_j(\mathbf{e}^{\text{TM}}, T, \mathbf{0}) &= k_{1,j}(T) (\theta^{\text{TM}})^2 + \left[-\frac{2}{3!} k_{1,j}(T) + k_{2,j}(T) \right] (\theta^{\text{TM}})^4 + \dots, \end{aligned}$$

respectively, which are resulting in

$$k_{1,j}(T) = \frac{1}{2} g_j^{(2)}(T), \quad (19)$$

$$k_{2,j}(T) = \frac{1}{3} k_{1,j}(T) + \frac{1}{4!} g_j^{(4)}(T), \quad (20)$$

etc. Using MA energy on the single R ion in Eq. (18), the total MA constants are obtained as

$$K_1(T) = \frac{1}{V_0} \sum_{j=1}^{n_R} k_{1,j}(T) + K_1^{\text{TM}}(T) \quad (p=1), \quad (21)$$

$$K_p^{(q)}(T) = \frac{1}{V_0} \sum_{j=1}^{n_R} k_{p,j}^{(q)}(T) \quad (p \geq 2), \quad (22)$$

where $K_p(T)$ and $K_p^q(T)$ are out-of-plane and in-plane MA constants in the whole system.

The orbital and spin components of the magnetic moment of a single- R ion in equilibrium can be calculated by

$$m_{L,j}(T, \mathbf{B}) = -\mu_B \sum_n \rho_{n,j}(T, \mathbf{B}) \langle n, j | \hat{L} | n, j \rangle, \quad (23)$$

$$m_{S,j}(T, \mathbf{B}) = -2\mu_B \sum_n \rho_{n,j}(T, \mathbf{B}) \langle n, j | \hat{S} | n, j \rangle, \quad (24)$$

respectively, where $\rho_{n,j}(T, \mathbf{B}) = \exp[-\beta E_{n,j}(\mathbf{e}_0^{\text{TM}}, \mathbf{B})]/Z_j(\mathbf{e}_0^{\text{TM}}, T, \mathbf{B})$, $|n, j\rangle$ is the n th eigenstate for $E_{n,j}(\mathbf{e}_0^{\text{TM}}, \mathbf{B})$, and

TABLE II. Probability weight for each J -multiplet calculated by $W_J(T)$ in Eq. (26). For $J = 13/2$ and $15/2$, $W_J(T) = 0.0$.

J	5/2	7/2	9/2	11/2
$T = 0$	0.93217	0.06548	0.00229	0.00005
$T = T_C$	0.90536	0.09049	0.00406	0.00009

the total magnetization $M_s(T, \mathbf{B})$ is given as

$$\mathbf{M}_s(T, \mathbf{B}) = \frac{1}{V_0} \sum_{j=1}^{n_R} \mathbf{m}_j(T, \mathbf{B}) + M^{\text{TM}}(T) \mathbf{e}_0^{\text{TM}}, \quad (25)$$

with $\mathbf{m}_j(T, \mathbf{B}) = \mathbf{m}_{L,j}(T, \mathbf{B}) + \mathbf{m}_{S,j}(T, \mathbf{B})$.

Finally, to confirm the convergence of the probability weights for excited- J multiplet states at $\mathbf{B} = \mathbf{0}$, we define the following weight function:

$$W_J(T) = \sum_{n,M} \rho_{n,j}(T, \mathbf{0}) |\langle n, j | J, M \rangle|^2. \quad (26)$$

In the case of SmFe₁₂ crystal, the value of $W_J(T)$ is independent of site index j . The results are shown in Table II, which indicates good convergence of weight for the number of excited J -multiplets even at $T = T_C = 555$ K. Thus in the calculation using the statistical method for SmFe₁₂, we take the excited J -multiplets up to $J = 9/2$. In the analytical calculation, the J -mixing effects are approximately treated only for the lowest- J multiplet by using unitary transformation.

B. Analytical method

According to the hierarchy of energy scale in R inter-metallic compounds, $\hat{H}_{\text{so}} \gg \hat{H}_{\text{ex}} \gg \hat{H}_{\text{CF}} \sim \hat{H}_{\text{Z}}$, we develop an analytical method for finite-temperature magnetic properties that enables us to connect the thermodynamic properties directly to our model parameters based on electronic states. Practically, we generalize the analytical expression of the Gibbs free energy [20,24] to include the effects of J -mixing using a first-order perturbation for the CF potential and Zeeman energy. We also derive an analytical expression for the magnetization curve, which enables us to estimate the CF potential using the observed results. The procedure of the formalism consists of (i) construction of a starting Hamiltonian for a single R ion, (ii) approximation for a diagonal matrix element of an effective Hamiltonian, (iii) finite-temperature perturbation for a single R ion, and (iv) thermodynamic analysis.

1. Effective lowest- J multiplet Hamiltonian for a single R ion

To restrict \hat{H}_R in low-energy subspace for $\hat{H}_{\text{so}} \gg \hat{H}_{\text{ex}}$, the effective lowest- J multiplet Hamiltonian $\hat{H}_R^{\text{eff},J}$ is obtained by unitary transformation and projection, where the off-diagonal matrix elements between inter- J multiplets become negligibly small, and a compensating term \hat{H}_{mix} is added in the diagonal element for the lowest- J multiplet. We introduce here a modified version of the effective Hamiltonian as explained below.

First, we define a rotational operator $\hat{D}(\mathbf{e}^{\text{TM}})$ that transforms the quantization axis to \mathbf{e}^{TM} . With this operator, the

Hamiltonian \hat{H}_R and \hat{H}_A ($A = \text{ex, CF, and Z}$) is transformed to

$$\hat{D}^\dagger(\mathbf{e}^{\text{TM}}) \hat{H}_R \hat{D}(\mathbf{e}^{\text{TM}}) \equiv \hat{H}'_R = \hat{H}'_{\text{so}} + \hat{H}'_{\text{ex}} + \hat{H}'_{\text{CF}} + \hat{H}'_{\text{Z}}, \quad (27)$$

$$\hat{H}'_{\text{so}} = \frac{\lambda}{2} [\mathbf{J}^2 - L(L+1) - S(S+1)], \quad (28)$$

$$\hat{H}'_{\text{ex}} = -2B_{\text{ex}}(T) C_0^{(1)}(\hat{S}), \quad (29)$$

$$\hat{H}'_{\text{CF}} = \sum_{l,m,m'} B_l^m \Theta_l^m [\mathcal{D}_{m,m'}^{(l)}(\mathbf{e}^{\text{TM}})]^* C_m^{(l)}(\hat{L}), \quad (30)$$

$$\begin{aligned} \hat{H}'_{\text{Z}} &= \mu_B \sum_{m,m'} b_{-m}^{(1)} [\mathcal{D}_{m,m'}^{(1)}(\mathbf{e}^{\text{TM}})]^* \\ &\times [C_m^{(1)}(\hat{L}) + 2C_m^{(1)}(\hat{S})], \end{aligned} \quad (31)$$

where $\hat{\mathbf{J}} = \hat{\mathbf{L}} + \hat{\mathbf{S}}$, $C_q^{(k)}(\hat{A})$ is the spherical tensor operator with rank k for angular momentum \hat{A} [50], and $b_m^{(1)}$ is a magnetic field tensor: $b_0^{(1)} = B_z$ and $b_{\pm 1}^{(1)} = -(\pm B_x + iB_y)/\sqrt{2}$. $\mathcal{D}_{m,m'}^{(l)}(\mathbf{e}^{\text{TM}}) = \mathcal{D}_{m,m'}^{(l)}(\varphi^{\text{TM}}, \theta^{\text{TM}}, 0)$ is Wigner's D function. Now we apply a unitary transformation (Schrieffer-Wolf transformation [52]) to \hat{H}'_R ,

$$e^{i\hat{\Omega}} \hat{H}'_R e^{-i\hat{\Omega}} = \hat{H}'_R + i[\hat{\Omega}, \hat{H}'_R] + O(\hat{\Omega}^2), \quad (32)$$

and we introduce a projection operator $\hat{P}_J = \sum_{M=-J}^J |J, M\rangle \langle J, M|$, by which the space of the J -multiplet is restricted to the lowest one. The operator $\hat{\Omega}$ is defined so as to remove the first-order off-diagonal matrix elements for J in \hat{H}'_R :

$$i \sum_{J'} [\hat{\Omega}, \hat{P}_J \hat{H}'_R \hat{P}_{J'}] = \sum_{J'} \hat{P}_J \hat{H}'_R \hat{P}_{J'} - \hat{H}'_R. \quad (33)$$

Apparently, $\langle J, M | \hat{\Omega} | J', M' \rangle = 0$. The second term on the right-hand side of Eq. (32) has now a diagonal matrix with corrections to the diagonal elements in the original \hat{H}'_R . The second- and higher-order terms in $\hat{\Omega}$ are neglected. By inserting Eq. (33) into Eq. (32), we obtain

$$\hat{H}_R^{\text{eff},J} = \hat{P}_J e^{i\hat{\Omega}} \hat{H}'_R e^{-i\hat{\Omega}} \hat{P}_J \equiv \hat{H}_R^J + \hat{H}_{\text{mix}}, \quad (34)$$

$$\hat{H}_R^J = \hat{P}_J \hat{H}'_R \hat{P}_J = E_J + \hat{H}_{\text{ex}}^J + \hat{H}_{\text{CF}}^J + \hat{H}_{\text{Z}}^J, \quad (35)$$

$$\hat{H}_{\text{mix}} = \frac{i}{2} \hat{P}_J [\hat{\Omega}, \hat{H}'_R] \hat{P}_J, \quad (36)$$

where $E_J = \lambda[J(J+1) - L(L+1) - S(S+1)]/2$ and $\hat{H}_A^J = \hat{P}_J \hat{H}'_A \hat{P}_J$ ($A = \text{ex, CF, and Z}$). We classify here analytical models depending on the approximation to the matrix element of $\hat{\Omega}$ for $J \neq J'$ in Eq. (33) as follows:

(i) Model A: Lowest- J multiplet without mixing as

$$\langle J, M | \hat{\Omega}^A | J', M' \rangle = 0.$$

(ii) Model B: Effective lowest- J multiplet with mixing as

$$\langle J, M | \hat{\Omega}^B | J', M' \rangle = i \frac{\langle J, M | \hat{H}'_1 | J', M' \rangle}{E_J - E_{J'}}.$$

(iii) Model C: Modified effective lowest- J multiplet with mixing (present study) as

$$\begin{aligned} \langle J, M | \hat{\Omega}^C | J', M' \rangle &= i \frac{\langle J, M | \hat{\mathcal{H}}_1 | J', M' \rangle}{E_{J'} - E_J} - \frac{i}{(E_{J'} - E_J)^2} \\ &\times \sum_{M''} [\langle J, M | \hat{\mathcal{H}}_1 | J', M'' \rangle \langle J', M'' | \hat{\mathcal{H}}_1 | J', M' \rangle \\ &- \langle J, M | \hat{\mathcal{H}}_1 | J, M'' \rangle \langle J, M'' | \hat{\mathcal{H}}_1 | J', M' \rangle], \end{aligned}$$

where $\hat{\mathcal{H}}_1 \equiv \hat{\mathcal{H}}'_R - \hat{\mathcal{H}}'_{so}$. The approximations are referred to as models A, B, and C hereafter. By using $\hat{\Omega}^B$, Magnani *et al.* derived the effective lowest- J multiplet Hamiltonian [29], and Kuz'min had also derived an equivalent approximation for anisotropy constants [28]. In the latter work, it was pointed out that the approximations of models A and B are not applicable to the Sm compounds due to relatively small λ . In the present study, we have modified $\hat{\Omega}^B$ to $\hat{\Omega}^C$.

2. Approximation for the diagonal matrix element of $\hat{\mathcal{H}}_R^{\text{eff}J}$

The energy levels for the $4f$ electron system are obtained by the exact diagonalization of $\hat{\mathcal{H}}_R$ in Eq. (6), and the diagonal matrix elements of $\hat{\mathcal{H}}_R^{\text{eff}J}$ can be expressed as

$$\langle J, M | \hat{\mathcal{H}}_R^{\text{eff}J} | J, M \rangle = \langle J, M | \hat{\mathcal{H}}'_R | J, M \rangle + \langle J, M | \hat{\mathcal{H}}_{\text{mix}} | J, M \rangle, \quad (37)$$

through two unitary transformations by $\hat{D}(e^{\text{TM}})$ and $e^{-\hat{\Omega}}$. The first term in Eq. (37) can be obtained by using the relation $\mathcal{D}_{m,0}^{(l)}(\varphi^{\text{TM}}, \theta^{\text{TM}}, 0) = Y_l^m(\theta^{\text{TM}}, \varphi^{\text{TM}})$ and the Wigner-Eckert theorem [50],

$$\begin{aligned} \langle J, M | \hat{\mathcal{H}}'_R | J, M \rangle &= E_J - 2(g_J - 1)\mu_B B_{\text{ex}}(T) \langle J, M | C_0^{(1)}(\hat{J}) | J, M \rangle \\ &+ \sum_{l,m} A_l^m \langle r^l \rangle \Theta_l^J \frac{t_l^m(e^{\text{TM}})}{a_{l,m}} \langle J, M | C_0^{(l)}(\hat{J}) | J, M \rangle \\ &+ \mu_B g_J (e^{\text{TM}} \cdot \mathbf{B}) \langle J, M | C_0^{(1)}(\hat{J}) | J, M \rangle, \end{aligned} \quad (38)$$

where Θ_l^J is the Stevens factor [46,53]. By using the model C with $\hat{\Omega}^C$, the second term in Eq. (37) is approximated as

$$\begin{aligned} \langle J, M | \hat{\mathcal{H}}_{\text{mix}} | J, M \rangle &\sim -\frac{1}{\Delta_{\text{so}}} \langle J, M | \hat{\mathcal{H}}'_{\text{ex}} | J+1, M \rangle \\ &\times \langle J+1, M | \hat{\mathcal{H}}'_{\text{ex}} + 2\hat{\mathcal{H}}'_{\text{CF}} + 2\hat{\mathcal{H}}'_Z | J, M \rangle \\ &\times \left[1 - \frac{\langle J+1, M | \hat{\mathcal{H}}'_{\text{ex}} | J+1, M \rangle - \langle J, M | \hat{\mathcal{H}}'_{\text{ex}} | J, M \rangle}{\Delta_{\text{so}}} \right], \end{aligned} \quad (39)$$

where $\Delta_{\text{so}} = \lambda(J+1)$. Contributions from $\hat{\mathcal{H}}'_{\text{CF}}$ and $\hat{\mathcal{H}}'_Z$ are neglected in the second term of the square bracket. By using the Wigner-Eckert theorem [50] and the relation for products of the matrix elements of the spherical tensor operators given by Eq. (5) in Chap. 12 of Ref. [51], the diagonal matrix

element is expressed as follows:

$$\begin{aligned} \langle J, M | \hat{\mathcal{H}}_{\text{mix}} | J, M \rangle &= -\Delta_{\text{ex}}(T) \frac{L+1}{3S} \langle J, M | \mathcal{T}_1(\hat{J}) | J, M \rangle \\ &- \sum_{l,m} A_l^m \langle r^l \rangle \Xi_l^J \frac{t_l^m(e^{\text{TM}})}{a_{l,m}} \frac{l(l+1)}{2l+1} \langle J, M | \mathcal{T}_l(\hat{J}) | J, M \rangle \\ &+ (e^{\text{TM}} \cdot \mathbf{B}) \frac{2(L+1)}{3(J+1)} \langle J, M | \mathcal{T}_1(\hat{J}) | J, M \rangle, \end{aligned} \quad (40)$$

where $\Delta_{\text{ex}}(T) = -2(g_J - 1)\mu_B B_{\text{ex}}(T)$. We use the relation $J = L - S$ assuming R as a light rare-earth element and $\Xi_6^J = -2^2/(3^3 \times 7 \times 11)$ and $-2^2 \times 17/(3^5 \times 7 \times 11^2)$ for Ce^{3+} and Sm^{3+} , respectively, and $\Xi_l^J = \Theta_l^J$ in the other cases.

More explicit expression of $\mathcal{T}_l(\hat{J})$ depends on further approximations. So far, two approximations have been adopted; one completely neglect the term $\langle J, M | \hat{\mathcal{H}}_{\text{mix}} | J, M \rangle$, that is, $\hat{\mathcal{H}}_{\text{mix}} = 0$ [24], and the other is an approximation to neglect the second term in the square brackets in Eq. (39), which was adopted by Kuz'min [28] and Magnani *et al.* [29]. According to the model approximations of $\hat{\Omega}^X$ with $X = A, B$, and C, the quantities $\mathcal{T}_l(\hat{J})$ are denoted as $\mathcal{T}_l^X(\hat{J})$ with $X = A, B$, and C. Clearly $\hat{\mathcal{T}}_l^A = 0$, and for $X = B$ and C,

$$\begin{aligned} \mathcal{T}_l^{\text{B(C)}}(\hat{J}) &= \frac{\Delta_{\text{ex}}(T)}{\Delta_{\text{so}}} \left[\frac{2J+l+1}{2} \mathcal{V}_{l-1}^{\text{B(C)}}(\hat{J}) \right. \\ &\left. - \frac{2}{2J+l+2} \mathcal{V}_{l+1}^{\text{B(C)}}(\hat{J}) \right], \end{aligned} \quad (41)$$

with

$$\begin{aligned} \mathcal{V}_l^{\text{B}}(\hat{J}) &= C_0^{(l)}(\hat{J}), \\ \mathcal{V}_l^{\text{C}}(\hat{J}) &= C_0^{(l)}(\hat{J}) + \frac{\Delta_{\text{ex}}(T) L + S + 1}{\Delta_{\text{so}}} \frac{1}{S(J+2)} \\ &\times \left[\frac{l(2J-l+1)(2J+l+1)}{4(2l+1)} C_0^{(l-1)}(\hat{J}) \right. \\ &\left. + \frac{l+1}{2l+1} C_0^{(l+1)}(\hat{J}) \right], \end{aligned} \quad (42)$$

where we formally set $C_0^{(-1)}(\hat{J}) = 0$.

The energy levels E_n for the $4f$ electron system, which consist of the lowest energy E_1 to the $2J$ th excited energy E_{2J+1} , are now expressed as

$$E_M^X = \langle J, M | \hat{\mathcal{H}}'_R | J, M \rangle + \langle J, M | \hat{\mathcal{H}}_{\text{mix}}^X | J, M \rangle \quad (43)$$

($X = A, B$, and C), with $M = -J$ to J for models A, B, and C.

Figure 3 shows the diagonal matrix element E_M^X ($X = A, B$, and C) of the effective lowest- J multiplet Hamiltonian $\hat{\mathcal{H}}_R^{\text{eff}J}$ at $T = 0$ in Eq. (43). Note that CF coefficients and exchange fields are determined by first-principles calculations, and the same values are used for models A, B, and C. The results are compared with the exact results. To distinguish the contribution from each $\hat{\mathcal{H}}_{so}$, $\hat{\mathcal{H}}_{\text{ex}}$, and $\hat{\mathcal{H}}_{\text{CF}}$ in $\hat{\mathcal{H}}_R$ of Eq. (6), the original Hamiltonian $\hat{\mathcal{H}}_R$ is taken as $\hat{\mathcal{H}}_{so}$, $\hat{\mathcal{H}}_{so} + \hat{\mathcal{H}}_{\text{ex}}$, or $\hat{\mathcal{H}}_{so} + \hat{\mathcal{H}}_{\text{ex}} + \hat{\mathcal{H}}_{\text{CF}}$.

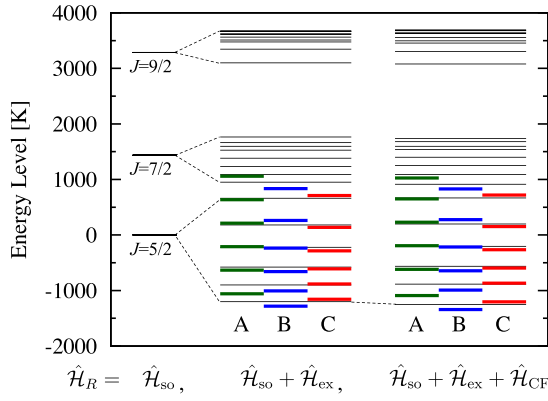


FIG. 3. Calculated energy levels of the Sm-4*f* states in SmFe₁₂ at $\mathbf{B} = \mathbf{0}$. Analytical results E_M^X with $X = A, B,$ and C for corresponding model approximations in Eq. (43) are given by thick green (A), blue (B), and red lines (C), respectively. To clarify the contributions from \hat{H}_{so} , \hat{H}_{ex} , and \hat{H}_{CF} , we take original Hamiltonian \hat{H}_R as $\hat{H}_R = \hat{H}_{so}$, $\hat{H}_{so} + \hat{H}_{ex}$, and $\hat{H}_{so} + \hat{H}_{ex} + \hat{H}_{CF}$. The numerically exact results are also shown by thin black lines.

Let us first describe the characteristics for the result $\hat{H}_R = \hat{H}_{so} + \hat{H}_{ex}$. In model A, the sixfold degeneracy of energy levels given by \hat{H}_{so} splits into equienergy levels as $E_M^A = E_J + \Delta_{ex}(0)M$. In model B, the equienergy levels shift to lower energy states by the J -mixing term, $E_M^B = E_J + \Delta_{ex}(0)M - |(J, M|\hat{H}_{ex}|J+1, M)|^2/\Delta_{so}$. In model C, the energy shifts, which were overestimates by the J -mixing term, are corrected.

The results obtained by $\hat{H}_R = \hat{H}_{so} + \hat{H}_{ex} + \hat{H}_{CF}$ show that the effect of CF potentials on the energy levels is weak, as expected, and they reproduce the results obtained by the numerical exact-diagonalization method as shown in Fig. 3.

3. Finite-temperature perturbation for a single *R* ion

We apply the first-order perturbation at finite temperature assuming $\hat{H}_{ex}^l \gg \hat{H}_{CF}^l + \hat{H}_Z^l + \hat{H}_{mix}^X$. The unperturbed and perturbed Hamiltonians are $\hat{H}_{ex}^l = \Delta_{ex}(T)C_0^{(1)}(\hat{\mathbf{J}}) \equiv \hat{H}^{(0)}$ and $\hat{H}_{CF}^l + \hat{H}_Z^l + \hat{H}_{mix}^X \equiv \hat{H}^l$, respectively. Note that \hat{H}_{so} is effectively taken into account in the J -multiplet formation of the R ion. The approximated Gibbs free energy for the R -4*f* partial system on the j th R site up to first-order perturbation is formally expressed as $g_j(\mathbf{e}^{\text{TM}}, T, \mathbf{B}) = -k_B \ln Z_0(T) + \sum_M \rho_M^{(0)}(T) \langle J, M | \hat{H}^l | J, M \rangle$, where $E_M^{(0)}(T) = \Delta_{ex}(T)M$, $Z_0(T) = \sum_M \exp[-\beta E_M^{(0)}(T)]$, and $\rho_M^{(0)}(T) = \exp[-\beta E_M^{(0)}(T)]/Z_0(T)$. More explicitly, it is given as

$$g(\mathbf{e}^{\text{TM}}, T, \mathbf{B}) = k_B T \sum_M \rho_M^{(0)}(T) \ln \rho_M^{(0)}(T) + \sum_M \rho_M^{(0)}(T) E_M \quad (44)$$

by using E_M in Eq. (43). It is noted that $g(\mathbf{e}^{\text{TM}}, T, \mathbf{B})$ is model-dependent because E_M is equal to E_M^A , E_M^B , or E_M^C , corresponding to the model adopted.

By using Helmholtz free energy $f(\mathbf{e}^{\text{TM}}, T)$ for the R -4*f* partial system, the Gibbs free energy in the modified effective lowest- J model is given as

$$g(\mathbf{e}^{\text{TM}}, T, \mathbf{B}) = f(\mathbf{e}^{\text{TM}}, T) - m(T) \mathbf{e}^{\text{TM}} \cdot \mathbf{B}, \quad (45)$$

$$m(T) = \mu_B \left[g_J J B_J^1(x) - \frac{2(L+1)}{3(J+1)} T_J^1(x) \right], \quad (46)$$

with

$$f(\mathbf{e}^{\text{TM}}, T) = k_B T \sum_M \rho_M^{(0)}(T) \ln \rho_M^{(0)}(T) + f_{ex}(T) + f_{CF}(\mathbf{e}^{\text{TM}}, T), \quad (47)$$

$$f_{ex}(T) = -\Delta_{ex}(T) \left[J B_J^1(x) + \frac{L+1}{3S} T_J^1(x) \right], \quad (48)$$

$$f_{CF}(\mathbf{e}^{\text{TM}}, T) = \sum_{l,m} A_l^m \langle r^l \rangle \Xi_l^m \frac{t_l^m(\mathbf{e}^{\text{TM}})}{a_{l,m}} \times \left[J^l B_J^l(x) + \frac{l(l+1)}{2l+1} T_J^l(x) \right]. \quad (49)$$

Here $x \equiv J \Delta_{ex}(T)/k_B T$, and the model dependence appears in $T_J^l(x)$, which is denoted as $T_J^{l,X}(x)$ with $X = A, B,$ or C . For $X = A$, $T_J^{l,A}(x) = 0$ and for $X = B$ and C ,

$$T_J^{l,B(C)}(x) = \frac{\Delta_{ex}(T)}{\Delta_{so}} \left[\frac{2J+l+1}{2} V_J^{l-1,B(C)}(x) - \frac{2}{2J+l+2} V_J^{l+1,B(C)}(x) \right], \quad (50)$$

with

$$V_J^{l,B}(x) = J^l B_J^l(x), \quad (51)$$

$$V_J^{l,C}(x) = J^l B_J^l(x) - \frac{\Delta_{ex}(T) L + S + 1}{\Delta_{so} S(J+2)} \times \left[\frac{l(2J-l+1)(2J+l+1)}{4(2l+1)} J^{l-1} B_J^{l-1}(x) + \frac{l+1}{2l+1} J^{l+1} B_J^{l+1}(x) \right], \quad (52)$$

where $B_J^l(x)$ is the generalized Brillouin function [24] defined by $(-1)^l J^l B_J^l(x) = \langle C_0^{(l)}(\hat{\mathbf{J}}) \rangle_0$ with $x = J \Delta_{ex}(T)/k_B T$ for $l \geq 0$, where $\langle \hat{A} \rangle_0 = \sum_M \rho_M^{(0)}(T) \langle J, M | \hat{A} | J, M \rangle$. The analytical expression of $B_J^l(x)$ is given in Ref. [29], and $T_J^{l,A}(x) = 0$, $T_J^{l,B}(x)$, and $T_J^{l,C}(x)$ are linear combinations of $B_J^{l-1}(x)$ and $B_J^{l+1}(x)$, and $B_J^{l-2}(x)$, $B_J^l(x)$, and $B_J^{l+2}(x)$, respectively, as shown in Eq. (50).

Because of the first-order perturbation for \hat{H}_Z^l , an analytical expression of the magnetic moment $m(T)$ is obtained as $m(T) = m_L(T) + m_S(T)$ with

$$m_L(T) = \mu_B \left[\frac{L+1}{J+1} J B_J^1(x) + \frac{2(L+1)}{3(J+1)} T_J^1(x) \right], \quad (53)$$

$$m_S(T) = -2\mu_B \left[\frac{S}{J+1} J B_J^1(x) + \frac{2(L+1)}{3(J+1)} T_J^1(x) \right], \quad (54)$$

where $m_L(T)$ and $m_S(T)$ are orbital and spin components of the magnetic moment on the R ion. It is noted that $m_L(T)$ and

$m_S(T)$ are model-dependent because of the model dependence of $T_J^l(x)$ as shown above.

Within the finite-temperature perturbation theory, the angular \mathbf{e}^{TM} -dependent part of single R ion free energy $f(\mathbf{e}^{\text{TM}}, T)$ in Eq. (47) with the tetragonal symmetry can be written as

$$\begin{aligned} f(\mathbf{e}^{\text{TM}}, T) = & k_1(T) \sin^2 \theta + [k_2(T) + k_2^1(T) \cos 4\varphi^{\text{TM}}] \\ & \times \sin^4 \theta^{\text{TM}} + [k_3(T) + k_3^1(T) \cos 4\varphi^{\text{TM}}] \\ & \times \sin^6 \theta^{\text{TM}} + C(T), \end{aligned} \quad (55)$$

which is a truncated form of $g(\mathbf{e}^{\text{TM}}, T, \mathbf{0})$ in Eq. (18). The $C(T)$ is an angle-independent constant. For example, the leading anisotropy constants for a trivalent magnetic light R ion (Ce^{3+} , Pr^{3+} , Nd^{3+} , Pm^{3+} , and Sm^{3+}) can be written as follows:

$$\begin{aligned} k_1(T) = & -3[J^2 B_J^2(x) + \frac{6}{5} T_J^2(x)] A_2^0 \langle r^2 \rangle \Xi_2^J \\ & - 40[J^4 B_J^4(x) + \frac{20}{9} T_J^4(x)] A_4^0 \langle r^4 \rangle \Xi_4^J \\ & - 168[J^6 B_J^6(x) + \frac{42}{13} T_J^6(x)] A_6^0 \langle r^6 \rangle \Xi_6^J, \end{aligned} \quad (56)$$

$$\begin{aligned} k_2(T) = & 35[J^4 B_J^4(x) + \frac{20}{9} T_J^4(x)] A_4^0 \langle r^4 \rangle \Xi_4^J \\ & + 378[J^6 B_J^6(x) + \frac{42}{13} T_J^6(x)] A_6^0 \langle r^6 \rangle \Xi_6^J. \end{aligned} \quad (57)$$

All terms of MA constants $k_p^{(q)}(T)$ in models A, B, and C are given by linear terms with respect to $A_l^m \langle r^l \rangle$.

We may rewrite the approximations used and adopted in the present formalism by using $T_J^{l,X}(x)$ in Eq. (50) as follows:

(i) Model A: Lowest- J multiplet without mixing as $\Delta_{\text{ex}}(T)/\Delta_{\text{so}} = 0$ or $T_J^{l,A}(x) = 0$ [24].

(ii) Model B: Effective lowest- J multiplet with mixing as $[\Delta_{\text{ex}}(T)/\Delta_{\text{so}}]^2 = 0$ or $T_J^{l,B}(x)$ [28,29].

(iii) Model C: Modified effective lowest- J multiplet with mixing as $T_J^{l,C}(x)$ (present study).

At $T = 0$, we have found that the following simple relation holds between $T_J^{l,C}(\infty)$ and $T_J^{l,B}(\infty)$ as

$$R_J = \frac{T_J^{l,C}(\infty)}{T_J^{l,B}(\infty)} = 1 - \frac{\Delta_{\text{ex}}(0)}{\Delta_{\text{so}}} \frac{(L+S+1)J}{S(J+2)}. \quad (58)$$

Because R_J is independent of l , relations among the models $X = A, B$, and C on $m_{L,S}^X(0)$ and $k_p^{(q),X}(0)$ can be generally expressed as follows:

$$m_{L,S}^C(0) = m_{L,S}^A(0) + R_J [m_{L,S}^B(0) - m_{L,S}^A(0)], \quad (59)$$

$$k_p^{(q),C}(0) = k_p^{(q),A}(0) + R_J [k_p^{(q),B}(0) - k_p^{(q),A}(0)]. \quad (60)$$

At finite temperatures, $T_J^{l,B(C)}(x)$ for $J = 5/2$ scaled by $T_J^{l,B}(\infty) > 0$ are shown in Fig. 4(a) for the SmFe_{12} compound. Here, $\Delta_{\text{ex}}(T)/\Delta_{\text{so}}$ is taken to be $0.206\alpha(T)$. For comparison purposes, we also show the $B_J^l(x)/B_J^l(\infty)$ in Fig. 4(b). $B_J^l(x)$ decays faster than $T_J^{l,B(C)}(x)$ with increasing temperature. Thus the J -mixing effects included in $T_J^{l,B(C)}(x)$ remain even at high temperatures.

4. Thermodynamic analysis

Finally, we investigate the thermodynamic instability by using the thermodynamic relation between Gibbs and

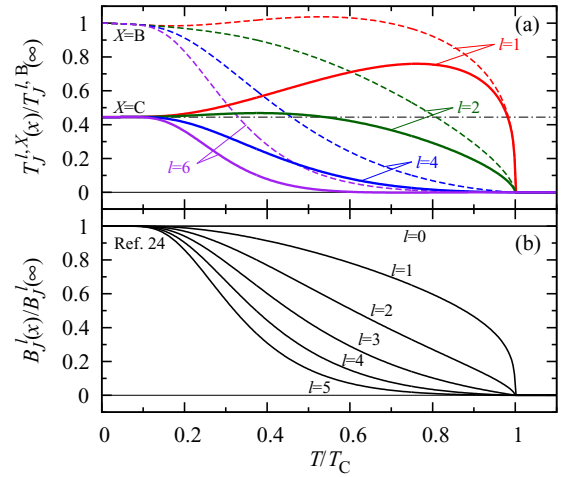


FIG. 4. Temperature dependence of (a) $T_J^{l,B(C)}(x)$ scaled by $T_J^{l,B}(\infty) > 0$ in Eq. (50) for model B (C) with broken (solid) curves, and (b) generalized Brillouin function $B_J^l(x)/B_J^l(\infty)$ [24] with $J = 5/2$ and $x = J\Delta_{\text{ex}}(T)/k_B$, where the temperature is scaled by Curie temperature T_C . The dashed-dotted line represent the value of R_J (see the text).

Helmholtz free energy, which explicitly contains the CF potentials and the exchange field determined by first-principles calculations. We have to note that above room temperature the exchange contribution $\hat{\mathcal{H}}_{\text{ex}}$ decreases with increasing temperature at a rate proportional to $\alpha(T)$, so the energy hierarchy is changed and thermal fluctuation effects have to be considered as $k_B T \gg \hat{\mathcal{H}}_{\text{CF}} \sim \hat{\mathcal{H}}_{\text{ex}}$. Even in this case, the formulation derived here based on the generalized Brillouin function holds, as shown by Kuz'min in Refs. [26,28]. In this thermodynamic analysis, we use model C.

By applying the finite-temperature perturbation theory to the lowest- J multiplet Hamiltonian, the approximated Gibbs free-energy density for the whole system can be expressed as

$$G(\mathbf{e}^{\text{TM}}, T, \mathbf{B}) = F(\mathbf{e}^{\text{TM}}, T) - \mathbf{M}_s(T) \cdot \mathbf{B}, \quad (61)$$

$$F(\mathbf{e}^{\text{TM}}, T) = \frac{1}{V_0} \sum_{j=1}^{n_R} f_j(\mathbf{e}^{\text{TM}}, T) + K_1^{\text{TM}}(T) \sin^2 \theta^{\text{TM}}, \quad (62)$$

$$\mathbf{M}_s(T) = \left[\frac{1}{V_0} \sum_{j=1}^{n_R} m_j(T) + M^{\text{TM}}(T) \right] \mathbf{e}^{\text{TM}}, \quad (63)$$

where $F(\mathbf{e}^{\text{TM}}, T)$ is the Helmholtz free-energy density for the whole system with model C, and $f_j(\mathbf{e}^{\text{TM}}, T)$ and $m_j(T)\mathbf{e}^{\text{TM}}$ are the corresponding energy for the $4f$ -shell, and the expectation value of the magnetic moment on the j th R ion given in Eqs. (47) and (46), respectively. The temperature dependence of $G(\mathbf{e}^{\text{TM}}, T, \mathbf{B})$ can be expressed as the linear combination of the generalized Brillouin functions for R ion $B_J^l(J\Delta_{\text{ex}}/k_B T)$ and the temperature coefficient for TM ion $\alpha(T)$ in Eq. (12). The equilibrium condition is the same as Eq. (17), where \mathbf{e}_0^{TM} becomes the direction of total magnetization in the equilibrium. We can also analyze the instability of magnetic metastable states, which are crucially important

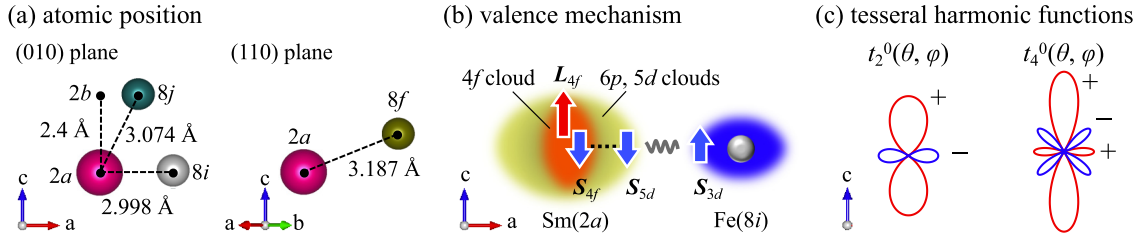


FIG. 5. (a) Atomic position of first- (8*i*), second- (8*j*), and third- (8*f*) neighbor Fe atoms of the Sm ion in SmFe₁₂, (b) illustration of the valence mechanism [56] in SmFe₁₂, and (c) typical tessellar harmonic functions as the basis of the CF Hamiltonian, where signs represent the phase.

in permanent magnetic materials. The metastable condition is $\delta G(T, \mathbf{e}^{\text{TM}}, \mathbf{B}) > 0$ for given T and \mathbf{B} with $|e^{\text{TM}}| = 1$.

The MA constants in the whole system are obtained by combining the contribution from the R sublattice in Eq. (55) with the Fe sublattice as in Eqs. (21) and (22). $K_1(T)$ can be substituted into the so called Krönmüller equation [54,55] to obtain the coercive field

$$B_c(T) = \alpha B_N(T) - N_{\text{eff}} M_s(T), \quad (64)$$

$$B_N(T) = \frac{2K_1(T)}{M_s(T)}, \quad (65)$$

where $B_c(T)$ and $B_N(T)$ are coercive and nucleation fields, respectively. α (< 1) is a microstructural parameter and N_{eff} is a local effective demagnetization factor [55]. The $B_N(T)$ gives the upper limit of $B_c(T)$.

IV. CALCULATED RESULTS FOR SmFe₁₂

A. Valence mechanism of magnetic anisotropy

We first calculate the charge-density distribution and the Coulomb potential at 0 K on constituent atoms of the SmFe₁₂ lattice (Fig. 1) using the first-principles calculations. The calculated results determine the values of CF acting on 4*f* electrons, the magnitude of the exchange field $B_{\text{ex}}(0)$ acting on the J , and the magnitude of TM sublattice magnetization. These values are used for parameter values in the model Hamiltonian. The contribution to the CF from the charge-density distribution inside (outside) the muffin-tine sphere radius is called the ‘‘valence (lattice) contribution’’ [41]. If the CF is dominated by the former contribution, we call the mechanism of the MA the ‘‘valence mechanism’’ [56].

The charge-density distributions of a single R ion are approximately replaced with charge density on atomic orbitals of 6*p* and 5*d* states. To evaluate the valence contribution to CF parameters $A_l^0(r^l)(\text{val})$, we introduce distribution parameters $\Delta n_{6p}^{(2)}$, $\Delta n_{5d}^{(2)}$ [57,58], and $\Delta n_{5d}^{(4)}$ defined as

$$\Delta n_{n'l'}^{(l)} = \frac{4\pi}{2l+1} a_{l,0} \sum_{m'} \int d\Omega t_l^0(\theta, \varphi) |t_{l'}^{m'}(\theta, \varphi)|^2 n_{n'l',m'}, \quad (66)$$

where Ω is the solid angle and m' indicates the multiple orbitals for the quantum number ($n'l'$). The shape of the function $t_l^0(\theta, \varphi)$ in Eq. (66) is given in Fig. 5(c).

The particular cases are as follows:

$$\Delta n_{6p}^{(2)} = \frac{1}{5} [n_{6p,z} - \frac{1}{2}(n_{6p,x} + n_{6p,y})], \quad (67)$$

$$\Delta n_{5d}^{(2)} = \frac{1}{7} [n_{5d,z^2} + \frac{1}{2}(n_{5d,xz} + n_{5d,yz}) - (n_{5d,x^2-y^2} + n_{5d,xy})], \quad (68)$$

$$\Delta n_{5d}^{(4)} = \frac{1}{28} [n_{5d,z^2} - \frac{2}{3}(n_{5d,xz} + n_{5d,yz}) + \frac{1}{6}(n_{5d,x^2-y^2} + n_{5d,xy})], \quad (69)$$

where $n_{n'l',m'}$ is the occupation number of the ($n'l', m'$) orbital. We note that $\Delta n_{6p}^{(4)} = 0$. Valence contributions of $A_2^0(r^2)$ and $A_4^0(r^4)$ are determined as [39,41]

$$A_2^0(r^2)(\text{val}) = F^{(2)}(4f, 6p)\Delta n_{6p}^{(2)} + F^{(2)}(4f, 5d)\Delta n_{5d}^{(2)}, \quad (70)$$

$$A_4^0(r^4)(\text{val}) = F^{(4)}(4f, 5d)\Delta n_{5d}^{(4)}, \quad (71)$$

with the Slater-Condon parameters

$$F^{(l)}(4f, n'l') = \frac{e^2}{4\pi\epsilon_0} \iint_0^{r_c} \frac{r_{<}^l}{r_{>}^{l+1}} r^2 |R_{4f}(r)|^2 r'^2 |R_{n'l'}(r')|^2 dr' dr > 0, \quad (72)$$

where $r_{<} = \min(r, r')$ and $r_{>} = \max(r, r')$. Via Eqs. (70) and (71), the distribution parameters $\Delta n_{n'l'}^{(l)}$ determine $A_l^0(r^l)(\text{val})$. It may be noted that no 6*p* and 5*d* orbitals exist for $A_6^0(r^6)(\text{val})$.

A simple explanation for the appearance of the uniaxial MA in a Sm ion surrounded by Fe atoms is given as follows. Figure 5(a) shows the lattice structure of SmFe₁₂ [10,30]. The left panel of Fig. 5(b) shows the location of Sm and Fe on the (010) plane of the lattice. Because of the short atomic distance between Sm and the first-nearest-neighbor (n.n.) Fe(8*i*) sites, the distribution of valence electrons on Sm extends within the a - b plane as shown in Fig. 5(c). According to the negative sign of $t_2^0(\theta, \varphi)$ in Fig. 5(d), the distribution parameters defined by Eq. (66) in terms of electron numbers of 6*p* and 5*d* orbitals are negative; $\Delta n_{6p}^{(2)} = -0.0012$, $\Delta n_{5d}^{(2)} = -0.0011$. Therefore, we obtain $A_2^0(r^2)(\text{val}) < 0$ by Eq. (70) in agreement with the numerical value of $A_2^0(r^2)$ shown in Table I. As shown by Eq. (56), the main contribution of the MA constant $k_1(T)$ is given by a product of A_2^0 and the positive value of Stevens factor Θ_2^0 , and $k_1(T)$ becomes positive. This means that $K_1(T) > 0$ because $K_1^{\text{TM}}(T) > 0$.

TABLE III. Magnetic moments $m_{L,S}(0)$ (μ_B) in Eqs. (53) and (54) and MA constants $k_{1,2}(0)$ (K) in Eqs. (56) and (57) for models A, B, and C at 0 K for a single Sm ion. Results obtained by Boltzmann statistics of $m_{L,S}(0, \mathbf{0})$ defined by Eqs. (23) and (24) and $k_{1,2}(0)$ defined by Eqs. (19) and (20) are also shown in the fifth column.

Model	A	B	C	Statistics
m_L	4.29	5.04	4.62	4.70
m_S	-3.57	-5.08	-4.24	-4.39
k_1	60.2	144.5	97.7	101.1
k_2	-14.0	-74.6	-40.9	-23.5

On the other hand, second-neighbor Fe(8*j*) and third-neighbor Fe(8*f*) atoms of the Sm atom are situated obliquely upward as shown in Fig. 5(b). According to the negative sign of $t_4^0(\theta, \varphi)$ shown in Fig. 5(d), we obtained $\Delta n_{sd}^{(4)} = -0.0013$ using Eq. (69), and $A_4^0\langle r^4 \rangle(\text{val}) < 0$ from Eq. (71). Again, the negative value is consistent with the numerical values of $A_4^0\langle r^4 \rangle$. The main contribution of MA constant $k_2(T)$ comes from a product of $A_4^0\langle r^4 \rangle$ and the positive value of Θ_4^0 , and results in $K_2(T) < 0$.

Thus, the sign of MA constants $K_1(T)$ and $K_2(T)$ are determined by the configuration of Sm and Fe atoms in the lattice. In the following, we investigate the J -mixing effect on single Sm magnetic properties at $T = 0$ K.

B. J -mixing effect and zero-temperature magnetic properties of SmFe₁₂

To clarify the J -mixing effect on single-ion magnetic properties, we show the calculated results of the magnetic moments $m_{L,S}(0)$ and the MA constants $k_{1,2}(0)$ for models A, B, and C in Table III. We used Eqs. (53) and (54) for $m_{L,S}(0)$ and Eqs. (56) and (57) for $k_{1,2}(0)$, and the values of $A_l^m\langle r^l \rangle$, $B_{\text{ex}}(0)$, and $M^{\text{TM}}(0)$ in Table I. As a reference, we also show the results obtained by the statistical method: $m_{L,S}(0, \mathbf{0})$ in Eqs. (23) and (24) and $k_{1,2}(0)$ defined in Eqs. (19) and (20). Both the analytical and statistical results give $k_1(0) > 0$ and $k_2(0) < 0$ for three models A, B, and C. The calculated results in model C (present model) agree best with the statistical ones.

We find that the absolute values of $m_{L,S}(0)$ and $k_{1,2}(0)$ in models B and C are larger than those in model A, which is attributed to inclusion of the J -mixing effects. The model B proposed in previous studies [28,29] overestimated the J -mixing effects by $1/R_J$ compared with model C, where $R_J = 0.44$ in Eq. (58) for SmFe₁₂. Actually, values of $m_{L,S}^C$ and $k_{1,2}^C$ in Table III satisfy the relation in Eq. (59) and (60). The results in the present study ($X = C$) agree quantitatively well with the statistical ones except for $k_2^C(0)$. The discrepancy in $k_2^C(0)$ may be due to omitting the second-order terms of $A_2^0\langle r^2 \rangle$ in Eq. (57), which have a positive contribution independent of the sign of $A_2^0\langle r^2 \rangle$ [25].

C. Finite-temperature magnetic properties of SmFe₁₂

We calculated the results of finite-temperature magnetic properties for a single Sm ion in equilibrium at $\mathbf{e}_0^{\text{TM}} = \mathbf{n}_c$: the magnetic moment $m_{L,S}(T)$ in Eqs. (53) and (54) and the

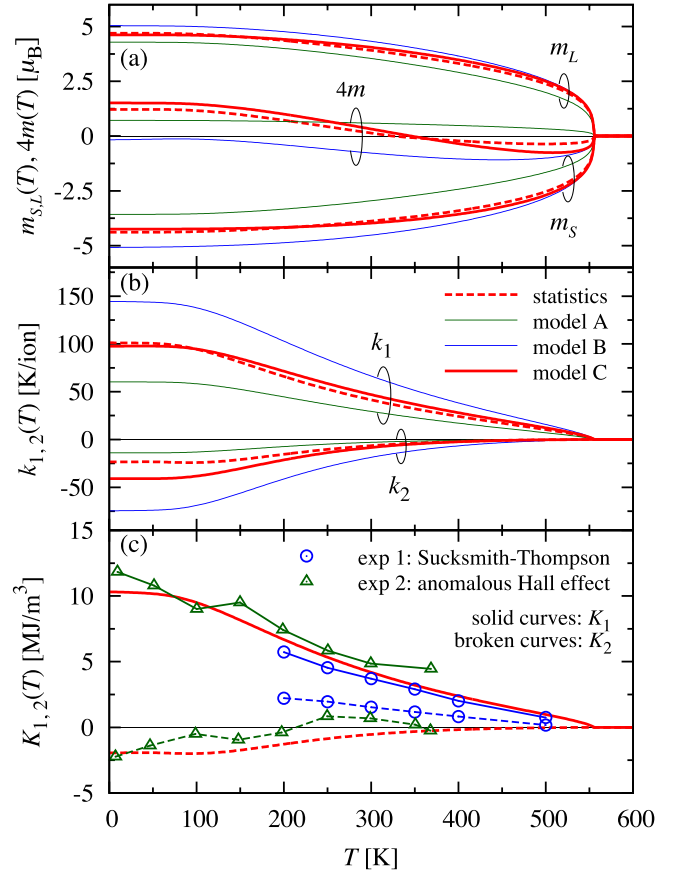


FIG. 6. Temperature dependence of (a) magnetic moments of Sm ion $m_{L,S}(T)$ and $m(T)$ at $\mathbf{B} = \mathbf{0}$ and (b) MA constants per single Sm ion $k_{1,2}(T)$ calculated by using models A, B, and C. Results obtained by Boltzmann statistics are shown by broken curves. (c) Temperature-dependent MA constants $K_{1,2}(T)$ in SmFe₁₂ by using the statistical method for Sm sublattice contribution $k_{1,2}(T)$, which are compared with experimental ones using the Sucksmith-Thompson (circles) [10] and the anomalous Hall effect (triangles) [12]. For both calculated and experimental results in (c), $K_1(T)$ and $K_2(T)$ are shown by solid and broken curves, respectively.

MA constants $k_{1,2}(T)$ in Eqs. (56) and (57) are shown in Figs. 6(a) and 6(b), respectively. The results show that the J -mixing effect in model B increases the absolute values of both $m_{L,S}(T)$ and $k_{1,2}(T)$. The overestimation in model B is modified by the present model C in the whole temperature range. The obtained results of model C reproduce well the statistical results for $m_{L,S}(T, \mathbf{0})$ in Eqs. (23) and (24) and for $k_{1,2}(T)$ in Eqs. (19) and (20) as shown by broken lines in Figs. 6(a) and 6(b).

The physical meaning of the increment of the absolute value of $m_{L,S}(T)$ and $k_{1,2}(T)$ by J -mixing may be given as follows. The expression of the free energy given by Eq. (48) includes the J -mixing effect in the second term of the square brackets. The term decreases $f_{\text{ex}}(x)$ by $-\mu_B B_{\text{ex}}(T) \delta S(T)$, where $\delta S(T) = \frac{2(L+1)}{3(J+1)} T_J^1(T) > 0$. Because of the decrease in $f_{\text{ex}}(x)$, the absolute value of the spin $\langle C_0^{(1)}(\hat{S}) \rangle_0$ and orbital moments $\langle C_0^{(1)}(\hat{L}) \rangle_0$ along \mathbf{e}_0^{TM} are increased by $\delta S(T)$. The tensor operators $\langle C_0^{(l)}(\hat{L}) \rangle_0$ for even l are also increased by

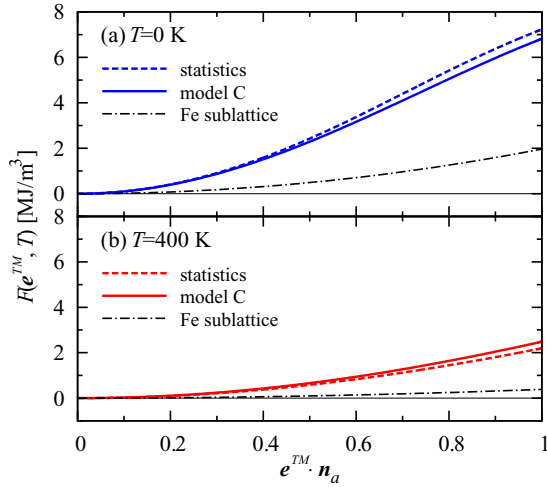


FIG. 7. Dependence of Helmholtz free-energy density on $e^{\text{TM}} \cdot \mathbf{n}_a$ with $e^{\text{TM}} \cdot \mathbf{n}_b = 0$ in SmFe_{12} at (a) $T = 0$ and (b) 400 K. Analytical results $F(e^{\text{TM}}, T)$ in Eq. (62) and results of $G(e^{\text{TM}}, T, \mathbf{0})$ obtained by Boltzmann statistics in Eq. (14) are shown by solid and broken curves, respectively, in which the contribution from Fe sublattice is included. The dashed-dotted curves represent the Fe sublattice MA energy: $K_1^{\text{TM}}(T)(e^{\text{TM}} \cdot \mathbf{n}_a)^2$.

$\frac{l(l+1)}{2l+1} T_J^l(x)$, which contribute to an increase in the absolute value of the MA constants $k_p^{(q)}(T)$.

The magnetic moment of Sm ion $m(T)$ is reversed at around $T_{\text{comp}} = 350$ K in model C and calculation by Boltzmann statistics. The temperature is called compensation temperature. This phenomenon is observed also in other Sm compounds [59,60]. Zhao *et al.* pointed out that this phenomenon also appears at $T = 337$ K in $\text{Sm}_2\text{Fe}_{17}\text{N}_x$ using the statistical method including similar parameter values to ours, such as $\mu_B B_{\text{ex}}(0)/k_B = 300$ K and $\lambda/k_B = 411$ K [61]. Their results are comparable with ours; however, the mechanism has not been surveyed. In the present model C, the magnetic moment of the Sm ion can be written as $m(T) = g_J \mu_B J B_J^1(x) - \mu_B \delta S(T)$. Because $\mu_B \delta S(T)$ is proportional to $T_J^{1,C}(x)$ and monotonically increasing with temperature below $T/T_C = 0.8$ as shown in Fig. 4(a), the term compensates for the $g_J \mu_B J B_J^1(x)$ at T_{comp} .

Figure 6(c) shows the results of $K_1(T)$ and $K_2(T)$ obtained by the statistical method in SmFe_{12} , which are compared with experimental ones denoted by exp 1 and exp 2 measured by the Sucksmith-Thompson method [10] and the anomalous Hall effect [12], respectively. In the whole temperature region, the results of $K_1(T)$ agree well with the experiments. Our statistical results qualitatively reproduce the experimental results below 200 K. The negative $K_2(T)$ at low temperatures is the origin of the first-order magnetization process (FOMP) as discussed below.

D. Thermodynamic properties of SmFe_{12}

Figure 7 shows calculated results of the Helmholtz free-energy density $F(e^{\text{TM}}, T)$ given in Eq. (62) for model C as a function of $e^{\text{TM}} \cdot \mathbf{n}_a$ with $e^{\text{TM}} \cdot \mathbf{n}_b = 0$ at $T = 0$ and 400 K, where $\mathbf{n}_{a(b)}$ is a unit vector parallel to the $a(b)$ -axis. The

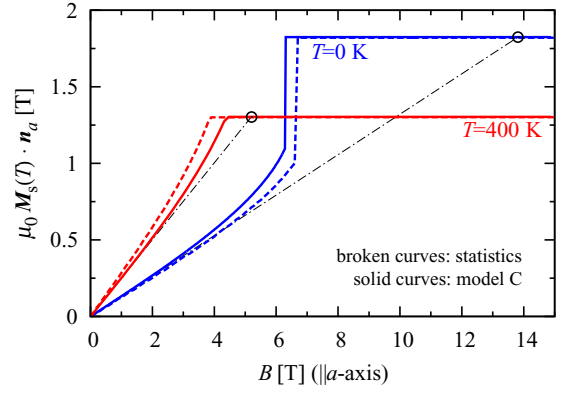


FIG. 8. Magnetization curves of SmFe_{12} at $T = 0$ and 400 K with applied field B parallel to the a -axis in the equilibrium calculated by analytical (solid curves) and statistical (broken curves) methods in Eqs. (63) and (25), respectively, where μ_0 is the magnetic constant. Dashed-dotted lines show tangent lines of magnetization curves at $B = 0$: $y = [\mu_0 M_s(T)]^2 / 2K_1 B$. Values of B at the circles correspond to the nucleation field $B_N(T)$ obtained by using the free-energy density of model C (see text).

results are compared with statistical ones of $G(e^{\text{TM}}, T, \mathbf{0})$ in Eq. (14). When the direction of e^{TM} is changed, the free-energy density on both Sm and Fe sublattices is increased. For the Sm sublattice, the energy increase originates from the CF, which can be expressed by the $\sum_j f_{\text{CF},j}(e^{\text{TM}}, T)$ in Eq. (55), and for the Fe sublattice, the energy increase can be written as $K_1^{\text{TM}}(T) \sin^2 \theta^{\text{TM}}$ with $K_1^{\text{TM}}(T) = 1.966$ and 0.387 MJ/m^3 at 0 and 400 K, respectively, which are much smaller than those of the Sm sublattice $\sum_j k_{1,j}(T)/V_0 = 8.059$ and 2.310 MJ/m^3 . The analytical results agree well with the statistical ones.

Figure 8 shows the calculated results of magnetization curves in the equilibrium states of SmFe_{12} at $T = 0$ and 400 K, where the magnetic field B is applied along the a -axis. Analytical results of the magnetization along the a -axis are compared with statistical ones. We have confirmed that the results in model C well reproduce the statistical ones. At $T = 0$, we find the characteristic behavior of an abrupt change in the magnetization $M_s(T) \cdot \mathbf{n}_a$ at $B = B_{\text{FP}}$. The change is called the first-order magnetization process, and the B_{FP} is called the FOMP field. At $T = 400$ K, no FOMP appears in both analytical and statistical results and the magnetization saturates at the MA field B_A . In SmFe_{12} , the magnetization curves at low temperatures were not reported; however, in $\text{SmFe}_{11}\text{Ti}$, the FOMP was observed at $T = 5$ K and $B_{\text{FP}} = 10$ T [6], which is qualitatively consistent with our results.

Let us consider the magnetization process along the c -axis and estimate nucleation field B_N in model C. The magnetization is first saturated as $M_s(T) \mathbf{n}_c$ along the c -axis by an infinitesimal field. Then the direction of the magnetic field is reversed and the magnitude is increased as $-\mathbf{Bn}_c$. The original state continues to exist as a quasistable state as far as the condition for a first-order variation $\delta G(\mathbf{n}_c, T, -\mathbf{Bn}_c) > 0$ is satisfied. The magnetization tends to decline when $\delta G(\mathbf{n}_c, T, -\mathbf{Bn}_c) = 0$. The applied magnetic field at which the latter condition is satisfied is the nucleation field, which has been given as $B_N = 2K_1(T)/M_s(T)$ [54].

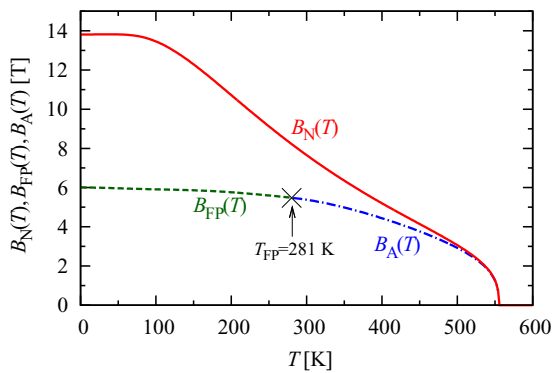


FIG. 9. Temperature dependence of the nucleation field $B_N(T)$, the MA field $B_A(T)$, and the FOMP field $B_{FP}(T)$ obtained by using the approximated free-energy density of model C neglecting $K_3(T)$, $K_2^1(T)$, and $K_3^1(T)$, the details of which are shown in Appendix. $B_{FP}(T)$ is the point of discontinuity in the FOMP realized below FOMP temperature T_{FP} (see the text).

Because B_N corresponds to the field at which the magnetization begins to decline with infinitesimal angle θ against the c -axis, the magnitude B_N in a realistic system can be estimated once the magnetization curve is obtained along a hard axis. Figure 8 shows the magnetization curve along the a -axis calculated in model C. B_N is given by a crossing point of the magnetization curve in the saturated state and the tangential line of the magnetization curve at zero field $y = [\mu_0 M_s(T)^2 / 2K_1(T)]$. When the value of $y = \mu_0 M_s$, the magnetic field coincides with B_N defined in Eq. (65).

The magnetization curves along the hard and easy axis in the case of $K_1(T) > 0$ and $K_2(T) < 0$ can be characterized by the nucleation field $B_N(T)$, the FOMP field $B_{FP}(T)$, and the MA field $B_A(T)$. These values are analytically expressed by using the ratio $\gamma(T) = K_1(T)/K_2(T)$ as

$$B_N(T) = \frac{2K_1(T)}{M_s(T)}, \quad (73)$$

$$B_{FP}(T) = B_N[x_{FP}(T) + 2\gamma(T)x_{FP}(T)^3] \quad [0 < x_{FP}(T) < 1], \quad (74)$$

$$B_A(T) = B_N[1 + 2\gamma(T)] \quad [x_{FP}(T) > 1], \quad (75)$$

with

$$x_{FP}(T) = \frac{1}{3} \left(-1 + \sqrt{-\frac{3}{\gamma(T)} - 2} \right), \quad (76)$$

where we use the approximate free-energy density: $F(\mathbf{e}^{\text{TM}}, T) = K_1(T) \sin^2 \theta^{\text{TM}} + K_2(T) \sin^4 \theta^{\text{TM}}$, in which the small contributions $K_3(T)$, $K_{2,3}^1(T)$ are neglected. Details are shown in Appendix. Calculated results of $B_N(T)$, $B_{FP}(T)$, and $B_A(T)$ are shown in Fig. 9. The condition of the FOMP appearance in model C is given by $-K_2(T) < K_1(T) < -6K_2(T)$ between $0 < x_{FP}(T) < 1$ in Eq. (74). As for SmFe_{12} , the FOMP is realized below $T = 281 \text{ K} \equiv T_{FP}$, which is analytically obtained from the condition $K_1(T) = -6K_2(T)$. The curves of $B_{FP}(T)$ and $B_A(T)$ are continuously connected at T_{FP} , which is referred to as the FOMP temperature. When $K_1(T) < -K_2(T)$, the magnetization direction is in-plane at $\mathbf{B} = \mathbf{0}$.

V. SUMMARY

The temperature dependence of magnetic anisotropy (MA) constants and magnetization of SmFe_{12} were investigated by using two methods for the model Hamiltonian, which combines quantum and phenomenological ones for rare-earth (R) and Fe subsystems, respectively. Parameter values of the R Hamiltonian were determined by first-principles calculations. The first method adopts a numerical procedure with Boltzmann statistics for the Sm $4f$ electrons. The other one is an analytical method that deals with the magnetic states of R ions with strong mixing of states with different quantum numbers of angular momentum J (J -mixing). We have modified the previous analytical methods for Sm ions, which have relatively small spin-orbit interaction, and we clarified that they overestimate the J -mixing effects for Sm transition-metal compounds. It has been shown that the results of our analytical method agree with those obtained by the statistical method. Our analytical method revealed that the increasing spin angular momentum with J -mixing caused by strong exchange field enhances the absolute value of orbital angular momentum and MA constants via spin-orbit interaction, and that these J -mixing effects remain even above room temperature. The calculated results of MA constants show that $K_1(T) > 0$ and $K_2(T) < 0$ in SmFe_{12} , in agreement with experiment.

The peculiar temperature dependence known as the first-order magnetization process (FOMP) in SmFe_{12} has been attributed to negative K_2 . It was also verified that the requirement for the appearance of FOMP is given as $-K_2 < K_1 < -6K_2$. The positive (negative) $K_{1(2)}$ appears due to an increase in the crystal-field parameter $A_2^0(r^2)$ ($A_4^0(r^4)$) caused by hybridization between $3d$ -electrons of Fe on the $8i$ ($8j$) site and $5d$ and $6p$ valence electrons on Sm. The mechanism of $K_1 > 0$ and $K_2 < 0$ in SmFe_{12} has thus been clarified by using the expressions of K_1 and K_2 obtained in the analytical method. Briefly, the sign of K_1 and K_2 in SmFe_{12} is attributed to the characteristic lattice structure around Sm ions, that is, crystallographic $2b$ -sites on the c -axis adjacent to Sm are vacant. We also present results on the magnetization process and nucleation fields by calculating the Gibbs free energy.

The present method will be applied to derive a general expression of the free energy to analyze MA of nonuniform systems such as disordered compounds, surfaces, and interfaces. The results will be reported in a forthcoming paper.

ACKNOWLEDGMENTS

This work was supported by the ElementsStrategy Initiative Center for Magnetic Materials (ESICMM), Grant No. JPMXP0112101004, through the Ministry of Education, Culture, Sports, Science and Technology (MEXT). T.Y. was supported by JSPS KAKENHI Grant No. JP18K04678. P.N. was supported by the project Solid21.

APPENDIX: MAGNETIZATION PROCESS IN THE CONDITION OF $K_1(T) > 0$ AND $K_2(T) < 0$

To investigate the magnetization process in equilibrium along the c -plane (e.g., the a -axis), we introduce the simplified model with magnetic anisotropy constants $K_1(T) > 0$ and $K_2(T) < 0$, which can be expressed by the Gibbs free energy

as

$$G(x, T, B) = K_1(T)x^2 + K_2(T)x^4 - BM_s(T)x \quad (|x| \leq 1), \quad (\text{A1})$$

where $x = \mathbf{M}_s(T) \cdot \mathbf{n}_a / M_s(T)$ with total magnetization \mathbf{M}_s and unit vector parallel to the a -axis \mathbf{n}_a . T and $\mathbf{B} = B\mathbf{n}_a$ ($B > 0$) are the temperature and the applied magnetic field, respectively. The equilibrium condition is

$$G(x_0, T, B) = \min_{|x| \leq 1} G(x, T, B),$$

where $x = x_0(T, B)$ gives the minimum of $G(x, T, B)$. For $K_1(T) \leq -K_2(T)$, the magnetization is always tilted to the a -axis direction due to $x_0(T, B) = 1$. Otherwise, the magnetization curve is given by

$$\mathbf{M}_s(T, B) \cdot \mathbf{n}_a = M_s(T)x_0(T, B). \quad (\text{A2})$$

The first-order magnetization process (FOMP) appears when $x_0(T, B)$ has two values at certain B , which is referred to as FOMP field B_{FP} .

To determine the $x_0(T, B)$ for $K_1(T) > -K_2(T)$, we show the first and second derivative of $G(x, T, B)$ with respect to x as

$$\frac{\partial G(x, T, B)}{\partial x} = 2K_1(T)x + 4K_2(T)x^3 - BM_s(T), \quad (\text{A3})$$

$$\frac{\partial^2 G(x, T, B)}{\partial x^2} = 2K_1(T) + 12K_2(T)x^2. \quad (\text{A4})$$

An inflection point of $G(x, T, B)$ for $x > 0$ at fixed T and B is given by $x_c(T) = \sqrt{-K_1(T)/6K_2(T)}$. Hereafter, we consider the following two cases: $x_c(T) \geq 1$ and $x_c(T) < 1$.

(i) The case of $x_c(T) \geq 1$.

$x_0(T, B)$ is obtained from the condition $\partial G(x, T, B)/\partial x = 0$ for $0 < x \leq 1$, because $\partial^2 G(x, T, B)/\partial x^2 > 0$ is always satisfied. The saturating point of magnetization $x_0(T, B) = 1$ is obtained from the condition $\partial G(x, T, B)/\partial x|_{x=1} = 0$ as

$$B = \frac{2K_1(T)}{M_s(T)}[1 + 2\gamma(T)] \equiv B_A(T), \quad (\text{A5})$$

where $\gamma(T) = K_2(T)/K_1(T)$. The B_A is the so-called anisotropy field.

(ii) The case of $x_c(T) < 1$.

$x_0(T, B)$ is obtained from the condition

$$G(x_0, T, B) = \min [G(x_e, T, B), G(1, T, B)], \quad (\text{A6})$$

where $x_e(T, B)$ is determined by the condition of local minimum as $\partial G(x, T, B)/\partial x = 0$ and $x_e(T, B) < x_c(T)$. In the magnetization process, $x_0(T, B)$ is continuously increased from zero with increasing B according to $x_0(T, B) = x_e(T, B)$ for $G(x_e, T, B) < G(1, T, B)$. At $B = B_{\text{FP}}$ such that $G(x_e, T, B) = G(1, T, B)$ is satisfied, $x_0(T, B)$ shows the abrupt jump and becomes a saturated value of $x_e(T, B) = 1$. The condition is rewritten as

$$(x_0 - 1)[3K_2(T)x_0^2 + 2K_2x_0 + K_1(T) + K_2(T)] = 0. \quad (\text{A7})$$

By solving Eq. (A7) for $0 < x_0 \leq 1$, two minimum points of $G(x, T, B)$ with respect to x are obtained at $x_0(T, B) = 1$ and

$$x_0(T, B) = \frac{1}{3} \left(-1 + \sqrt{-\frac{3}{\gamma(T)} - 2} \right) \equiv x_{\text{FP}}(T). \quad (\text{A8})$$

By using $x_{\text{FP}}(T)$, the field at which the FOMP occurs is determined by

$$B = \frac{2K_1(T)}{M_s(T)} [x_{\text{FP}}(T) + 2\gamma(T)x_{\text{FP}}(T)^3] \equiv B_{\text{FP}}(T). \quad (\text{A9})$$

As a result, for $-1 < \gamma(T) < -1/6$, the FOMP occurs between $\mathbf{M}_s(T) \cdot \mathbf{n}_a = M_s(T)x_{\text{FP}}(T)$ and $M_s(T)$.

-
- [1] T. Miyake, K. Terakura, Y. Harashima, H. Kino, and S. Ishibashi, *J. Phys. Soc. Jpn.* **83**, 043702 (2014).
- [2] Y. Hirayama, Y. K. Takahashi, S. Hirose, and K. Hono, *Scr. Mater.* **95**, 70 (2015).
- [3] G. C. Hadjipanayis, A. M. Gabay, A. M. Schönhöbel, A. Martín-Cid, J. M. Barandiarán, and D. Niarchos, *Engineering* **6**, 141 (2020).
- [4] K. Ohashi, Y. Yokoyama, R. Osugi, and Y. Tawara, *IEEE Trans. Magn.* **MAG-23**, 3101 (1987).
- [5] K. Ohashi, Y. Tawara, R. Osugi, and M. Shimao, *J. Appl. Phys.* **64**, 5714 (1988).
- [6] B.-P. Hu, H.-S. Li, J. P. Gavigan, and J. M. D. Coey, *J. Phys.: Condens. Matter* **1**, 755 (1989).
- [7] T. Kuno, S. Suzuki, K. Urushibara, K. Kobayashi, N. Sakuma, M. Yano, A. Kato, and A. Manabe, *AIP Adv.* **6**, 025221 (2016).
- [8] A. M. Schönhöbel, R. Madugundo, O. Yu. Vekilova, O. Eriksson, H. C. Herper, J. M. Barandiarán, and G. C. Hadjipanayis, *J. Alloys Compd.* **786**, 969 (2019).
- [9] H. Kato, T. Nomura, M. Ishizone, H. Kubota, and T. Miyazaki, *J. Appl. Phys.* **87**, 6125 (2000).
- [10] Y. Hirayama, Y. K. Takahashi, S. Hirose, and K. Hono, *Scr. Mater.* **138**, 62 (2017).
- [11] D. Ogawa, X. D. Xu, Y. K. Takahashi, T. Ohkubo, S. Hirose, and K. Hono, *Scr. Mater.* **164**, 140 (2019).
- [12] D. Ogawa, T. Yoshioka, X. D. Xu, Y. K. Takahashi, H. Tsuchiura, T. Ohkubo, S. Hirose, and K. Hono, *J. Magn. Mater.* **497**, 165965 (2020).
- [13] H. Sepelri-Amin, Y. Tamazawa, M. Kambayashi, G. Saito, Y. K. Takahashi, D. Ogawa, T. Ohkubo, S. Hirose, M. Doi, T. Shima, and K. Hono, *Acta Mater.* **194**, 337 (2020).
- [14] R. F. L. Evans, W. J. Fan, P. Chureemart, T. A. Ostler, M. O. A. Ellis, and R. W. Chantrell, *J. Phys.: Condens. Matter* **26**, 103202 (2014).
- [15] Y. Toga, M. Matsumoto, S. Miyashita, H. Akai, S. Doi, T. Miyake, and A. Sakuma, *Phys. Rev. B* **94**, 174433 (2016).
- [16] M. Nishino, Y. Toga, S. Miyashita, H. Akai, A. Sakuma, and S. Hirose, *Phys. Rev. B* **95**, 094429 (2017).

- [17] T. Miyake and H. Akai, *J. Phys. Soc. Jpn.* **87**, 041009 (2018).
- [18] T. Yoshioka and H. Tsuchiura, *Appl. Phys. Lett.* **112**, 162405 (2018).
- [19] H. Tsuchiura, T. Yoshioka, and P. Novák, *Scr. Mater.* **154**, 248 (2018).
- [20] M. Yamada, H. Kato, H. Yamamoto, and Y. Nakagawa, *Phys. Rev. B* **38**, 620 (1988).
- [21] R. Sasaki, D. Miura, and A. Sakuma, *Appl. Phys. Express* **8**, 043004 (2015).
- [22] D. Miura, R. Sasaki, and A. Sakuma, *Appl. Phys. Express* **8**, 113003 (2015).
- [23] D. Miura and A. Sakuma, *AIP Adv.* **8**, 075114 (2018).
- [24] M. D. Kuz'min, *Phys. Rev. B* **46**, 8219 (1992).
- [25] M. D. Kuz'min and J. M. D. Coey, *Phys. Rev. B* **50**, 12533 (1994).
- [26] M. D. Kuz'min, *Phys. Rev. B* **51**, 8904 (1995).
- [27] Y. Millev and M. Fähnle, *Phys. Rev. B* **52**, 4336 (1995).
- [28] M. D. Kuz'min, *J. Appl. Phys.* **92**, 6693 (2002).
- [29] N. Magnani, S. Carretta, E. Livioti, and G. Amoretti, *Phys. Rev. B* **67**, 144411 (2003).
- [30] Y. Harashima, K. Terakura, H. Kino, S. Ishibashi, and T. Miyake, *JPS Conf. Proc.* **5**, 011021 (2015).
- [31] W. Körner, G. Krugel, and C. Elsasser, *Sci. Rep.* **6**, 24686 (2016).
- [32] P. Delange, S. Biermann, T. Miyake, and L. Pourovskii, *Phys. Rev. B* **96**, 155132 (2017).
- [33] J. H. Van Vleck, *The Theory of Electric and Magnetic Susceptibilities* (Oxford University Press, Oxford, 1932).
- [34] S. G. Sankar, V. U. S. Rao, E. Segal, W. E. Wallace, W. G. D. Frederick, and H. J. Garrett, *Phys. Rev. B* **11**, 435 (1975).
- [35] H. W. de Wijn, A. M. van Diepen, and K. H. J. Buschow, *Phys. Status Solidi B* **76**, 11 (1976).
- [36] H. Sepehri-Amin, T. Ohkubo, T. Nishiguchi, S. Hirokawa, and K. Hono, *Scr. Mater.* **63**, 1124 (2010).
- [37] H. Sepehri-Amin, T. Ohkubo, S. Nagashima, M. Yano, T. Shoji, A. Kato, T. Schrefl, and K. Hono, *Acta Mater.* **61**, 6622 (2013).
- [38] P. Blaha, K. Schwarz, G. K. H. Madsen, D. Kvasnicka, and J. Luitz, *WIEN2k, An Augmented Plane Wave + Local Orbitals Program for Calculating Crystal Properties*, Karlheinz Schwarz (TU Wien, Austria, 2001).
- [39] M. Richter, P. M. Oppeneer, H. Eschrig, and B. Johansson, *Phys. Rev. B* **46**, 13919 (1992).
- [40] P. Novák, *Phys. Status Solidi B* **198**, 729 (1996).
- [41] K. Hummler and M. Fähnle, *Phys. Rev. B* **53**, 3272 (1996).
- [42] M. Richter, *J. Phys. D* **31**, 1017 (1998).
- [43] M. Diviš, K. Schwarz, P. Blaha, G. Hilscher, H. Michor, and S. Khmelevskiy, *Phys. Rev. B* **62**, 6774 (2000).
- [44] M. Diviš, J. Ruzs, H. Michor, G. Hilscher, P. Blaha, and K. Schwarz, *J. Alloys Compd.* **403**, 29 (2005).
- [45] M. Brooks, L. Nordström, and B. Johansson, *J. Phys. Condens. Mater* **3**, 3393 (1991).
- [46] M. T. Hutchings, *Solid State Phys.* **16**, 227 (1964).
- [47] R. J. Elliott, *Magnetic Properties of Rare Earth Metals* (Plenum, New York, 1972), Chap. 1.
- [48] M. D. Kuz'min, *Phys. Rev. Lett.* **94**, 107204 (2005).
- [49] S. A. Nikitin, I. S. Tereshina, V. N. Verbetskii, and A. A. Salamova, *Phys. Solid State* **40**, 258 (1998).
- [50] A. R. Edmonds, *Angular Momentum in Quantum Mechanics* (Princeton University Press, Princeton, NJ, 1960).
- [51] D. A. Varshalovich, A. N. Moskalev, and V. K. Khersonskii, *Quantum Theory of Angular Momentum* (World Scientific, Singapore, 1988).
- [52] J. R. Schrieffer and P. A. Wolff, *Phys. Rev.* **149**, 491 (1966).
- [53] K. Stevens, *Proc. Phys. Soc.* **A65**, 209 (1952).
- [54] H. Kronmüller, K. D. Drust, and M. Sagawa, *J. Magn. Magn. Mater.* **69**, 149 (1987).
- [55] H. Kronmüller and M. Fähnle, *Micromagnetism and the Microstructure of Ferromagnetic Solids* (Cambridge University Press, Cambridge, 2003).
- [56] H. Tsuchiura, T. Yoshioka, and P. Novák, *IEEE Trans. Magn.* **50**, 2105004 (2014).
- [57] R. Coehoorn, K. H. J. Buschow, M. W. Dirken, and R. C. Thiel, *Phys. Rev. B* **42**, 4645 (1990).
- [58] A. Sakuma, *J. Phys. Soc. Jpn.* **61**, 4119 (1992).
- [59] H. Adachi, H. Ino, and H. Miwa, *Phys. Rev. B* **56**, 349 (1997).
- [60] H. Adachi and H. Ino, *Nature (London)* **401**, 148 (1999).
- [61] T. S. Zhao, X. C. Kou, R. Grössinger, and H. R. Kirchmayr, *Phys. Rev. B* **44**, 2846 (1991).